Physics of the Earth and Planetary Interiors, 36 (1984) 236–259
Elsevier Science Publishers B.V., Amsterdam – Printed in The Netherlands

The role of a heterogeneous inclusion during continental collision

J.P. Vilotte [1,3], M. Daignieres [1], R. Madariaga [2] and O.C. Zienkiewicz [3]

[1] *Centre Géologique et Géophysique, Université des Sciences et Techniques du Languedoc, Place E. Bataillon, 34060 Montpellier Cedex (France)*

[2] *L.E.G.S.P., L.A. du CNRS no. 195, Institut de Physique du Globe, Universités Paris VI et VII, 4. place Jussieu, 75230 Paris Cedex 05 (France)*

[3] *Civil Engineering Department, University College of Swansea, Singleton Park, Swansea SA2 8PP (Gt. Britain)*

(Received November 17, 1983; revision accepted June 20, 1984)

Vilotte, J.P., Daignieres, M., Madariaga, R. and Zienkiewicz, O.C., 1984. The role of a heterogeneous inclusion during continental collision. Phys. Earth Planet. Inter., 36: 236–259.

We study a simple model of the deformation due to collision between two continental plates. The model is patterned after the geometry of the India–Asia collision but it may be applicable to more general situations. The collision is modelled by the indentation of a viscoplastic plate (Asia) by a rigid punch (India). A finite element approach, capable of dealing with finite deformation, heterogeneity and non linear rheologies is used to study the role of an inclusion of increased rigidity on the viscoplastic flow of the plate. The heterogeneous zone was chosen to approximate the shape and position of the Tarim basin behind Tibet. The lateral boundaries of the plate were defined so as to approximate those that are believed to apply for the Asian plate, i.e., fixed boundaries to the West and North, free boundaries to the West and South. Several geometries and contrasts of rheology were analyzed to verify the general validity of our results. The purpose was to determine the main kinematic features of the flow not to model the particular case of Tarim. It is found that the heterogeneity affects the flow in a drastic way even for small contrasts of rigidity and for small size heterogeneities. The main effect of the heterogeneity is to create two important shear zones or internal boundary layers. The most important is in front of the inclusion separating the main flow from the inclusion. As the flow proceeds, the inclusion rotates and the shear zone progressively bends in qualitative agreement with the bending of the large strike slip faults like the Altyn Tagh that separates the Tarim from Tibet. Our model of continuous deformation does not allow for the formation of faults or fractures, but the shear zones may be understood as the initial stages for the generation of fractures or velocity discontinuities. Another shear zone develops to the left of the inhomogeneity, near the fixed boundary and in the wake of the punch. The role of these shear zones is to isolate the heterogeneity from the main flow to facilitate its rigid rotation inside the flow of the softer plate. A final observation is that in the presence of the heterogeneity the lower left hand corner rotates almost like a rigid block producing a sharp bend on the left hand side of the plate. As the inclusion rotates pushed by the punch this rigid block rotates clockwise to open up the space necessary for the homogeneity.

1. Introduction

In a previous work, Vilotte et al. (1982) presented a numerical method to solve the problem of the plane indenter under plane strain or plane stress conditions, and for a variety of lithospheric rheologies. The technique was applied to the study of intracontinental deformation, in particular to the collision between India and Asia (Tapponnier and Molnar, 1976). The model that was studied was extremely simplified because our main concern was to analyse the effect of boundary conditions and deformation mode (plane stress or plane strain) on the evolution of the indented plate. Among the simplifications that were introduced we think that the most important were: (1) the effect of gravity was not taken into consideration, (2) only infinitesimal deformation was studied;

0031-9201/84/$03.00

and (3) the lithosphere was assumed to be homogeneous. Those approximations are restrictive for the study of the complete geological evolution of this model of continental collision. As part of a continuing effort to study systematically the role of different parameters on continental deformation, we study here the effect of relaxing the last two restrictions cited above. The role of gravity will be reported elsewhere.

We consider the effect of a lithospheric heterogeneity upon the finite deformation of a plate indented by a rigid punch. The model parameters will be chosen so as to determine the effect of a rigid zone of the lithosphere in front of the indenter. Our intention is to approximate roughly the geometry of the Tarim depression to the North of Tibet. These models will be solved by a finite elements technique which allows us to take into account rheological heterogeneities and several types of boundary conditions and geometries. The evolution of the lithospheric plate is followed during finite deformation so that the continuum mechanical equations are solved on an updated version of the initial finite element grid. This allows us to study the deformation of the plate during a period of up to 35 Ma. Recent studies by Tapponnier et al. (1982) on a plasticine model confirmed the importance of following the finite deformation during the indenting of the punch. The finite elements formulation adopted is such that all the assumptions about rheology are clearly and explicitly introduced. We adopt a viscoplastic incompressible averaged lithospheric rheology, and we study only a plane strain model with a free lateral boundary condition. For this particular geometry Vilotte et al. (1982) demonstrated that the differences with plane stress deformation are not important. We study first a model with a homogeneous lithosphere, that serves as a reference for the analysis of the results obtained for lithospheres containing heterogeneities of different contrasts of rigidity and size.

2. The geophysical problem

The importance of intercontinental collisions on the geodynamic evolution and large scale deformation of the continental lithosphere has been extensively discussed in recent years. The deformation of rather large intracontinental domains may be traced back to the interaction between lithospheric plates. Such a geodynamically coherent framework has been proposed for several recent orogenic zones; for instance, for the alpine evolution of Asia (Tapponnier and Molnar, 1976) and the Mediterranean (Tapponnier, 1977). Intercontinental collision has also been considered for more ancient orogenies, like the Precambrian evolution of the Pan-African chain (Caby et al., 1980).

A number of different techniques to analyse continental collision quantitatively have been proposed; see, for instance, Tapponnier (1978), Daignières et al. (1978), England and McKenzie (1982, 1983), Vilotte et al. (1982). In all these studies the lithosphere was assumed to be homogeneous within the scale of the model. It is clear, however, that at these scales, of the order of 5000 km, the lithosphere may not be considered to be mechanically homogeneous; some blocks of different ages and structures should present different rigidities. The nature of these blocks may be different, for instance there may be remanent oceanic domains which were not subducted because of complex geometry, great sedimentary thickness, or age of the basins. These mechanical inclusions will present a different rheology from that of the surrounding lithosphere. These types of heterogeneities seem to be common in the Mediterranean (Tapponnier, 1977). They may also be of continental origin but of older ages. In fact, the continental lithosphere seems to form by the successive accretion of ancient blocks which may behave later as rigid inclusions. An example of such an evolution may be found in Asia, where the present continental plate appears to be the result of the accretion of several continental fragments around the Siberian platform. A particular example that will interest us here is the Tarim basin which appears to be an old shield, accreted during an older collision probably of Palaeozoic origin (Molnar and Tapponnier, 1981). The seismicity and recent deformation of the Tarim basin are very small as would be expected for a relatively rigid inclusion inside a plate subjected to large, active deformation. This difference in rheology may be due to

either strain hardening due to a complex history of deformation, or to colder temperatures which reduce the deformability of the plate.

We do not consider here the micromechanisms that lead to an increase rigidity of certain blocks of the lithosphere. We simply assume the existence of such blocks which we believe to be common, and we then study their effect upon the deformation and the state of stress of the lithosphere during the collision process.

3. The mechanical problem

3.1. Kinematics and rheology

We study the progressive evolution of the deformation due to the plane indentation of a viscoplastic incompressible plate. This plate is assumed to contain an internal block of increased rigidity. The mode of deformation is assumed to be plane strain. The mechanical formulation of the problem was discussed by Vilotte et al. (1982), where it was stressed that the strain and stress are considered as averaged over a certain volume of the lithosphere. Therefore, the stresses and strains that we model are not those that may be measured at a point but are representative values for the average over a finite block of the lithosphere. The elastic deformations are considered to be negligible when compared to the finite plastic deformations. We do not consider either the curvature of the plates. Under these approximations, we may write the transformation velocity gradient for a viscoplastic rheology in the form proposed by Mandel (1971)

$$\text{grad } \mathbf{v} = \dot{R}R^{\mathrm{T}} + \gamma\langle\phi(F)\rangle\frac{\partial F}{\partial \sigma} \tag{1}$$

where $\mathbf{v}$ is the particle velocity vector, R is the finite rotation of the point under consideration. This rotation is the same that is usually calculated during elastic deformation. While the elastic strain may be considered to be negligible, the rotation of an element in the vicinity of the current point may not be neglected. The last term in (1) represents the plastic strain velocity

$$\dot{\epsilon}^{\mathrm{P}}_{ij} = \gamma\langle\phi(F)\rangle\frac{\partial F}{\partial \sigma_{ij}} \tag{2}$$

where γ is the mean fluidity of the lithosphere, the angle brackets $\langle\rangle$ mean that

$$\langle\phi(F)\rangle = \phi(F) \quad \text{if } F \geqslant 0$$

and

$$\langle\phi(F)\rangle = 0 \quad \text{if } F < 0$$

F is the flow surface $F(\underline{\underline{\sigma}}, \underline{\underline{\dot{\epsilon}}}^p, \underline{\underline{\epsilon}}^p)$, a function of the stress $\underline{\underline{\sigma}}$, the plastic strain velocity $\underline{\underline{\dot{\epsilon}}}^p$ and the finite deformation $\underline{\underline{\epsilon}}^p$. Here, we adopt the von Mises criterion

$$F(\underline{\underline{\sigma}}) = \sqrt{3}\sqrt{J_2} - \sigma_y\left(\underline{\underline{\dot{\epsilon}}}^p, \underline{\underline{\epsilon}}^p\right) \tag{3}$$

where J_2 is the second invariant of the stress tensor

$$\sqrt{2}\sqrt{J_2} = (s_{ij}s_{ij})^{1/2}$$

with s_{ij} the deviatoric part of σ_{ij}. σ_y is the mean flow limit of the continental lithosphere (Vilotte et al., 1982). When $F(\underline{\underline{\sigma}}) < 0$ there is no deformation, the lithosphere is rigid while for $F(\underline{\underline{\sigma}}) \geqslant 0$ it flows plastically. The function $\phi(F)$ is the creep law which will be assumed to be of the power law type: $\phi(F) = F^n$.

With the latter assumption we may define an average viscosity (Zienkiewicz, 1977)

$$\mu = \frac{\sigma_y \pm \left(I_2/\gamma\sqrt{3}\right)^{1/n}}{I_2} \tag{4}$$

where I_2 is the second invariant of the strain velocity tensor, which for an incompressible medium is

$$I_2 = \sqrt{3}\,(\dot{\epsilon}_{ij}\dot{\epsilon}_{ij})^{1/2}$$

Note that I_2 is often written $\dot{\epsilon}$ in the mechanical literature.

With the preceding definitions and approximations it may be shown that the symmetric part of (1) is purely incompressible plastic, i.e.

$$\{\text{grad } \mathbf{v}\}_{ij} = \dot{\epsilon}^p_{ij} = \gamma F^n\left(\underline{\underline{\sigma}}, \underline{\underline{\dot{\epsilon}}}^p, \underline{\underline{\epsilon}}^p\right)\left(\frac{\sqrt{3}}{2\sqrt{J_2}}\right)s_{ij} \tag{5}$$

while the antisymmetric part of (1) yields

$$\}\text{grad } \mathbf{v}\{ = \underline{\underline{\dot{R}}}\underline{\underline{R}}^T = \underline{\underline{\dot{\omega}}} \tag{6}$$

where $\dot{\omega}$ is the vorticity. The notation $\{\}$ and $\}\{$ for the symmetric and antisymmetric parts of the

gradient of the velocity was introduced by Mandel (1971).

3.2. *Modelling*

To carry out a systematic study with a minimum number of free parameters we simplify the geometry of the problem and the boundary conditions. We study a rectangular plate (see Fig. 1) indented by a rigid rectangular punch moving at a constant speed u_0. The boundary AD is always rigid ($v_x = v_y = 0$) while DC is free to lateral slip ($v_y = 0$, v_x free). The AMNB and BC segments of the boundary are free so that $\underline{\underline{\sigma}} \cdot \hat{n} = 0$ where $\hat{n}$ is the external normal of the boundary. Following Tapponnier and Molnar (1976), the boundary condition BC closely reproduces the conditions at the subduction zones to the east of Tibet.

Two geometries are studied to establish the effect of the free boundaries on the evolution of the deformation. In the first model, shown in Fig. 1a, we put the BC boundary at an initial distance of 1.7 L to the right of the punch, where L is the width of the indenter. In the second model (fig. 1b) this boundary is at a distance L from the punch.

Given this initial geometry and the rheology as described by eq. 5 we determine the velocity field $\mathbf{v}(\mathbf{x}, t)$ and the stress tensor $\underline{\underline{\sigma}}(\mathbf{x}, t)$ from the equations of equilibrium

$$\operatorname{div} \underline{\underline{\sigma}}(\mathbf{x}, t) = 0 \tag{7}$$

The constitutive relationship

$$s_{ij}(\mathbf{x}, t) = 2\mu(\mathbf{x}, t)\dot{\epsilon}_{ij}(\mathbf{x}, t) \tag{8}$$

where μ is defined by (4). The flow is assumed to be incompressible, so that

$$\operatorname{div} \mathbf{v}(\mathbf{x}, t) = 0 \tag{9}$$

The boundary conditions are:

$$\mathbf{v} = \tilde{u}(\mathbf{x}) \quad \text{on } \Gamma_v(t)$$

and

$$\underline{\underline{\sigma}} \cdot \hat{\mathbf{n}} = c \quad \text{on } \Gamma_t(t) \tag{10}$$

where Γ_v and Γ_t designate, respectively, those segments of the boundary where velocities or stresses are specified.

The problem posed above gives the instantaneous field at time t for a given geometry of the plate. Since we want to integrate the deformation over several tens of million years, we also have to calculate the rotation $R(t + \Delta t)$ from (6) and up-

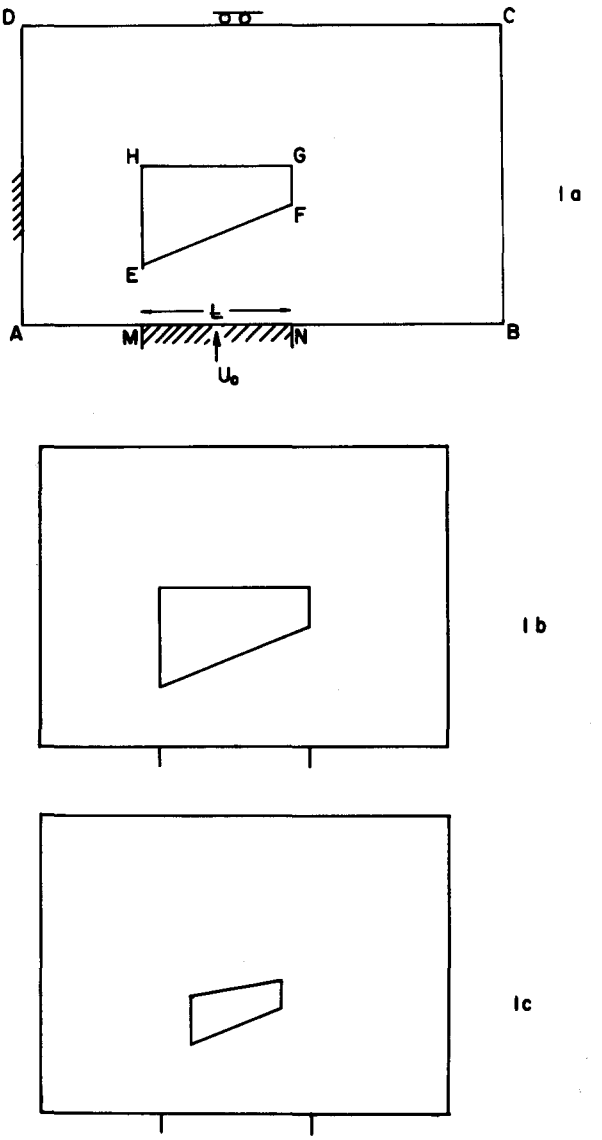

Fig. 1. Geometry of the models. Side AD has a zero velocity boundary conditions, DC is free to glide laterally and BC is free of stress. On AM and NB, stress-free boundary conditions are used, while the indenter is simulated by a fixed velocity boundary condition. In all calculations $u_0 = 5$ cm y^{-1}, MN = 2400 km. In (a) NB = 1.7 MN; (b) NB = MN; (c) NB = MN. EFGH represents the rheological heterogeneity.

date the geometry of the plate. The integration in time may be done explicitly or implicitly, the former procedure is simpler but requires a short time step to insure stability. A discussion of different ways to integrate the equation may be found in Zienkiewicz (1977) or in Vilotte et al. (in preparation).

We assume plane strain incompressible flow conditions i.e.

$$\dot{\epsilon}_{xz} = \dot{\epsilon}_{yz} = \dot{\epsilon}_{zz} = 0 \tag{11a}$$

and

$$\sigma_{zz} = \tfrac{1}{2}(\sigma_{xx} + \sigma_{yy}) = \sigma_p \tag{11b}$$

A geophysical justification of this approximation when the role of gravity is neglected has been proposed by Tapponnier (1978) and discussed in detail by Vilotte et al. (1982) who showed that for free boundary conditions along BC, the plane stress and plane strain solutions differ only in details. The problem has been solved by a finite element technique based on a reduced Galerkin formulation of eqs. 7–11. For details see Zienkiewicz (1977) and Vilotte (1983).

3.3. *Physical parameters and definition of the heterogeneity*

To make a systematic study of the problem and to establish the role of the different parameters we have to make a dimensional analysis of the equations. Let L be the width of the punch, u_0 its velocity of penetration, then we scale lengths by L, velocities by u_0 and time by L/u_0. All kinematical variables are scaled in this form, for instance, strain velocity scales like u_0/L.

For the dynamical variables we have a choice, either we scale stresses by the characteristic stress related to creep flow or by the yield stress σ_y. We introduce the following non-dimensional numbers

$$K = \sigma_y \left(\frac{\sqrt{3}\,\gamma L}{u_0} \right)^{1/n}$$

or

$$\bar{K} = \left(\frac{u_0}{\sqrt{3}\,L\gamma} \right)^{1/n} \frac{1}{\sigma_y} = K^{-1} \tag{12}$$

so that in the first case (see Vilotte et al., 1982) we have

$$s'_{ij} = s_{ij} \left(\frac{\sqrt{3}\,\gamma L}{u_0} \right)^{1/n}$$

and

$$\mu' = \left(K I_2^{-1} + I_2^{1/n-1} \right) \tag{13}$$

or in the second one

$$s'_{ij} = s_{ij}/\sigma_y$$

and

$$\mu' = \left(I_2^{-1} + \bar{K} I_2^{1/n-1} \right) \tag{14}$$

where primed quantities are non-dimensional. The choice of either normalization depends on the phenomenon that one wants to stress. If the interest is on the effect of creep on the plastic solution, the first formulation is to be preferred; while for the study of the effect of the yield stress on the solution, the second normalization should be adopted.

The heterogeneity that we have studied is indicated in Fig. 1 by the quadrilateral block EFGH. Since the block has a different rheology from that of the rest of the plate, the non-dimensional analysis has to be carried further. While the kinematic scaling is not affected the dynamic scaling defined by (13) or (14) has to be reconsidered. Let $\sigma_1 = u_0/\sqrt{3}\,\gamma_1 L$ be the characteristic stress corresponding to the plate, and $\sigma_2 = u_0/\sqrt{3}\,\gamma_2 L$ the characteristic stress of the heterogeneity.

Under the first normalization, that of (13), we adopt

$$s'_{ij} = s_{ij}/\sigma_1$$

and

$$\mu'_1 = \left(K_1 I_2^{-1} + I_2^{1/n-1} \right) \tag{15}$$

$$\mu'_2 = \left(\frac{\gamma_1}{\gamma_2} \right)^{1/n} \left(K_2 I_2^{-1} + I_2^{1/n-1} \right)$$

For the second normalization, that of (14), we designate $\sigma_y^{(1)}$ and $\sigma_y^{(2)}$ the yield stresses of the plate and the heterogeneities, respectively.
Then

$$s'_{ij} = s_{ij}/\sigma_y^{(1)}$$

and

$$\mu_1' = \left(I_2^{-1} + \bar{K}_1 I_2^{1/n-1}\right) \tag{16}$$

$$\mu_2' = \frac{\sigma_y^{(2)}}{\sigma_y^{(1)}}\left(I_2^{-1} + \bar{K}_2 I_2^{1/n-1}\right)$$

In (15) and (16) K_1, $\bar{K}_1$, K_2, $\bar{K}_2$ define the values of the non-dimensional parameters in (12) for the plate and the inclusion, respectively.

The parameter γ that defines the creep rheology of the plate and the heterogeneity is given by an average across the lithosphere

$$\gamma = \frac{1}{H}\int_0^H \gamma_0^L \, e^{-Q/RT} dz \tag{17}$$

where H is the lithospheric thickness. For a given geotherm and fixed lithospheric depth

$$\gamma = \frac{\gamma_0}{T_L - T_c}\left[T e^{-Q/RT} + \frac{Q}{T} E_1\left(\frac{Q}{RT}\right)\right]_{T_c}^{T_L} \tag{18}$$

Here, γ_0 is a constant, Q is the creep activation energy, E_1 the exponential integral, T_L and T_c the temperature at the base of the lithosphere and at the surface, respectively.

As discussed by Vilotte et al. (1982), γ changes rapidly as a function of the geotherm that is adopted. For an old shield, like the Tarim depression, we expect it to be colder and, therefore, that γ be smaller than for the surrounding lithosphere, i.e., that the shield be less "fluid" than the surrounding tectonically active areas. As an example, for a difference of 200°C at the base of the lithosphere, we get $(\gamma_1/\gamma_2)^{1/n} \approx 2.5 \times 10^2$ for a dry dunite rheology. Similarly, the yield stress σ_y depends on the history of deformation of the plate. In fact, if the medium has already been subjected to plastic flow it should contain large residual stress heterogeneities which in turn reduce the average yield stress for the new deformation period. Then the shields appear more rigid than the recently deformed, tectonically young areas that surround it. Both effects on the fluidity of the lithosphere, thermal or mechanical, are closely related. The two formulations (15) and (16) put the emphasis on either one of these effects.

Putting $\gamma_1 = \gamma_2$ in (15) we define the rheological contrast

$$R_1 = \frac{\sigma_y^{(2)}}{\sigma_y^{(1)}} \quad \text{for } n \text{ constant} \tag{19}$$

Similarly, putting $\sigma_y^{(1)} = \sigma_y^{(2)}$ we introduce

$$R_2 = \left(\frac{\gamma_1}{\gamma_2}\right)^{1/n} \quad \text{for } n \text{ constant} \tag{20}$$

The actual situation in a lithospheric heterogeneity should be intermediate between the two. In the following we study the effect of a rigid block for different values of the contrast R. To better establish the order of magnitude of the results we adopt the following physical dimensions: $L = 2400$ km, $u_0 = 5$ cm y^{-1}, $n = 3$, $\sigma_y^{(1)} = 30$ GPa, $\gamma_1 = 2.74 \times 10^{-37}$ s^{-1} Pa^{-3}, i.e., the non-dimensional parameters $K_1 = 2.69$ and $\bar{K}_1 = 0.37$. The dimension of the heterogeneity may be determined from Fig. 1 and its rheology is defined by the ratio: $R_1 = 10, 5, 2.5, 1$ for $\gamma_1 = \gamma_2$ as in (19). We have done a similar study of the effect of differences in γ_2. We also calculated for $\sigma_y^{(1)} = \sigma_y^{(2)}$ and $R_2 = 2.5 \times 10^2$. While the two types of heterogeneity are not entirely equivalent because of the non-linear nature of the problem, we find that the solutions differ only on details and that all the essential features of the flow depend in fact on the numerical value of R_1 or R_2.

4. Results for the homogeneous plate

Finite elements technique is used to solve this problem. The plate is divided into 88 quadratic Lagrangian elements. At every time step a non linear system of equations is solved using a Newton–Raphson technique and a frontal solver, when the solution has converged, we used the velocity field to update the mesh. The time step is chosen to be less than the Courant number and we check the mesh to avoid ill-deformed element.

We discuss the results of our numerical experiments by means of contour plots of the octahedral shear strain rate I_2 (the second invariant of the shear strain rate tensor), the pressure p and the vorticity $\dot{\omega}$. We prefer to plot these quantities rather than the velocity field (Fig. 2) because of the clearer information contained in the plot of space derivatives of the velocity field (I_2 and $\dot{\omega}$). The localisations of shear strain, the curvature of the deformation, etc. appear more clearly in these contour plots. The finite elements formulation per-

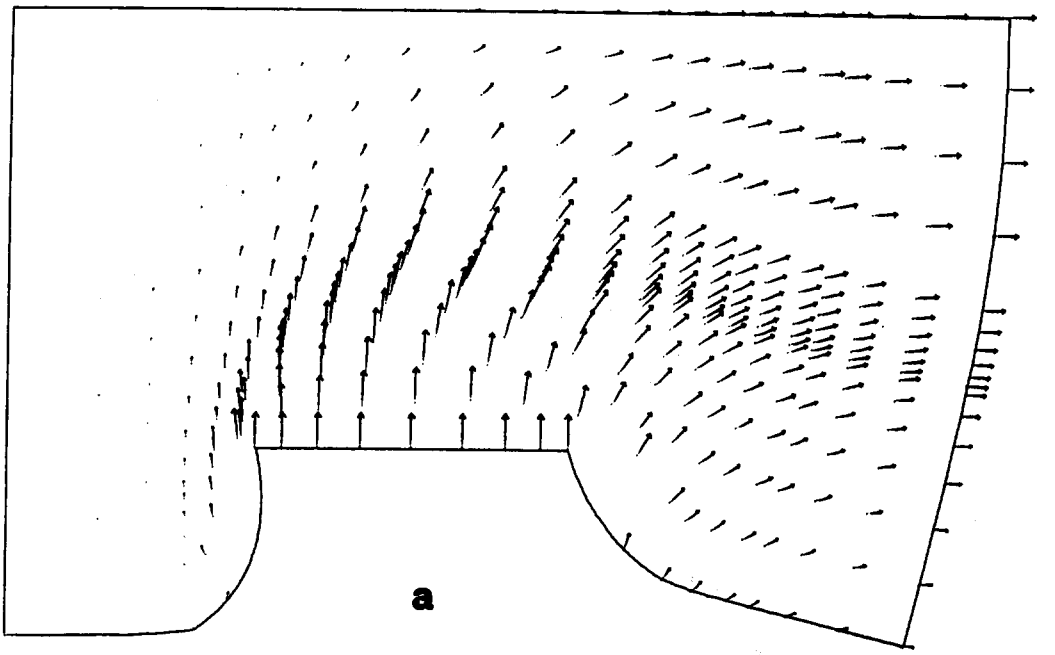

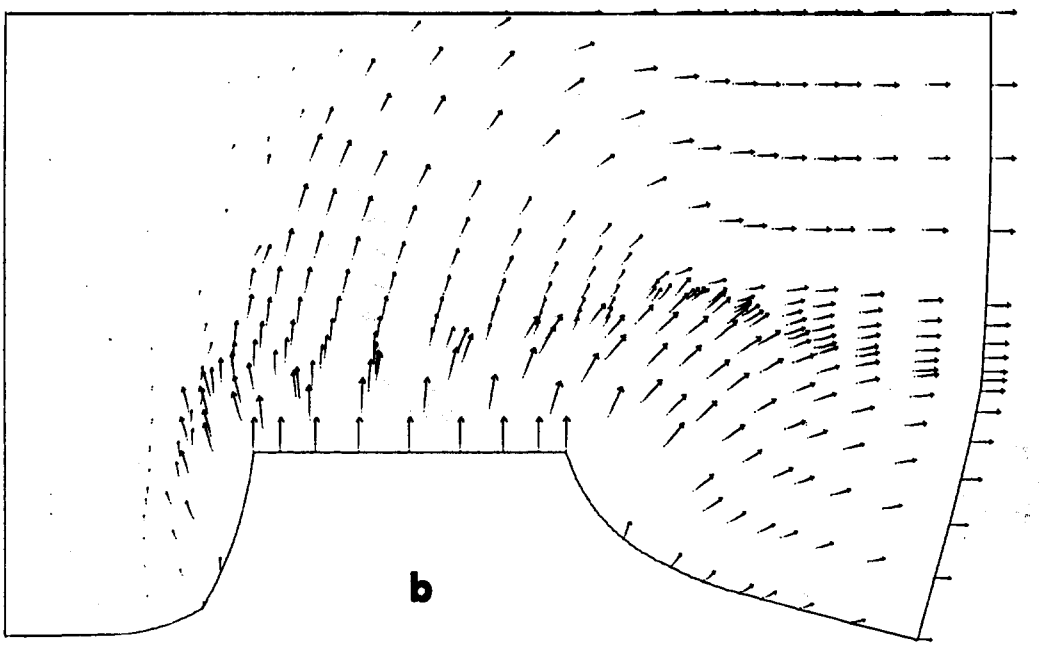

Fig. 2. Velocity field calculated for 2 of the numerical simulations. (a) Homogeneous model with NB = MN at 30 Ma; $R_1 = 1$. (b) Heterogeneous model with NB = MN at 30 Ma; $R_1 = 10$.

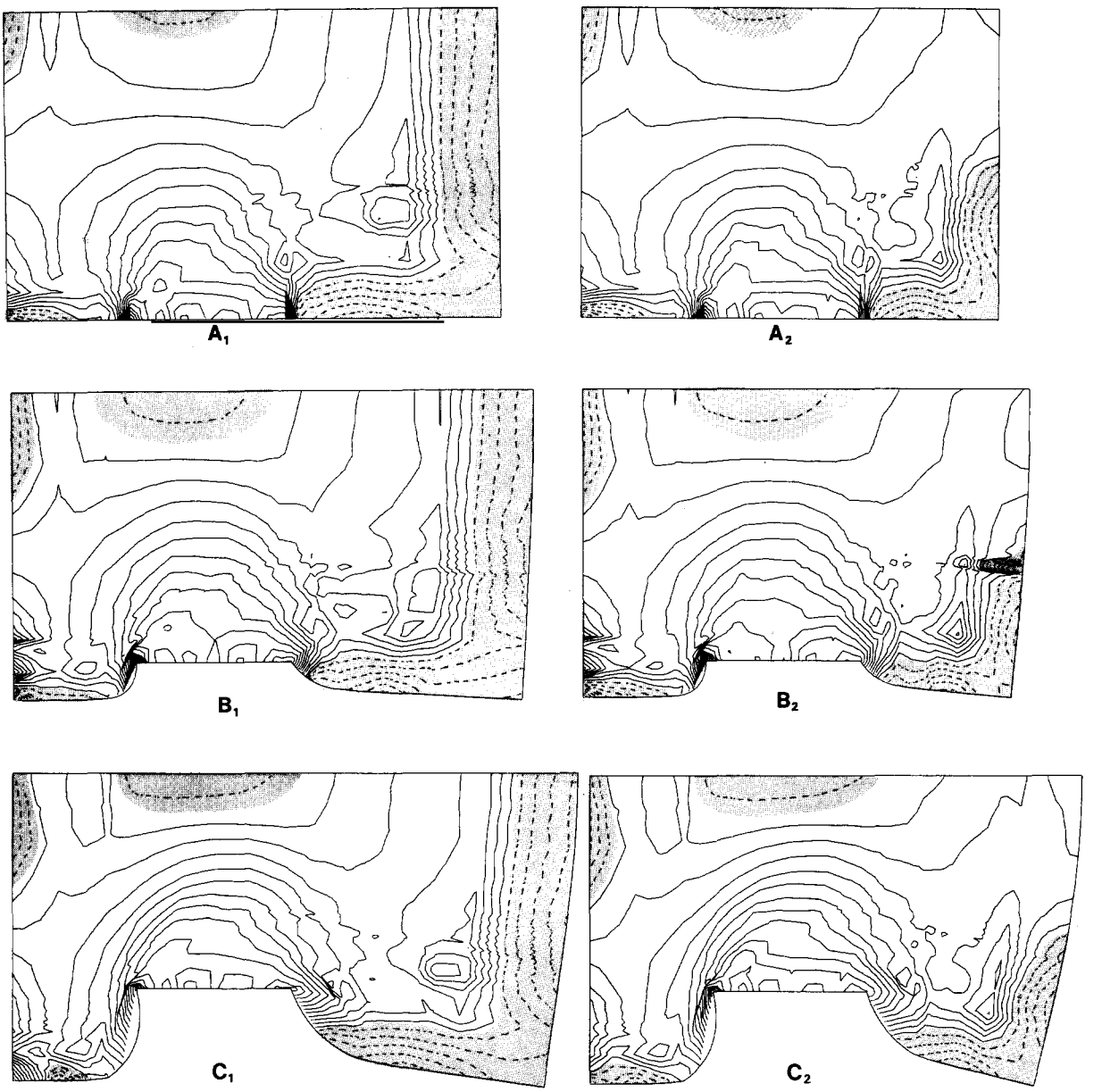

Fig. 3.(a) Pressure field for the homogeneous plate model. Dashed contour lines are used for negative pressure. A_1, B_1, C_1 are solutions for the model of Fig. 1a at $t = 0$, 15 and 30 Ma; A_2, B_2, C_2 are solutions for the model of Fig. 1b at the same times. Contour lines are plotted with a spacing of = 1.1 non-dimensional units. Extreme values for the pressure are, for A_1 ($P_{max} = 16.2$, $P_{min} = -4.7$), B_1 ($P_{max} = 18.3$, $P_{min} = -8$), C_1 ($P_{max} = 16.15$, $P_{min} = -4.71$) and for A_2 ($P_{max} = 16.9$, $P_{min} = -5.8$), B_2 ($P_{max} = 18.35$, $P_{min} = -8$) and C_2 ($P_{max} = 16.2$, $P_{min} = -3.6$). (b) Octahedral shear strain rates for the homogeneous plate model (see Fig. 3a for a definition of each frame). Contour lines are plotted with a spacing of 0.6 non-dimensional units, and the extreme values for A_1 are ($I_{2_{max}} = 10.9$, $I_{2_{min}} = 0.33 \times 10^{-3}$), for B_1 ($I_{2_{max}} = 12.3$, $I_{2_{min}} = 0.33 \times 10^{-3}$), C_1 ($I_{2_{max}} = 11.8$, $I_{2_{min}} = 0.33 \times 10^{-3}$), A_2 ($I_{2_{max}} = 10.5$, $I_{2_{min}} = 0.32 \times 10^{-3}$), B_2 ($I_{2_{max}} = 11$, $I_{2_{min}} = 0.33 \times 10^{-3}$) and C_2 ($I_{2_{max}} = 11.5$, $I_{2_{min}} = 0.33 \times 10^{-3}$). (c) Vorticity for the homogeneous plate model, negative vorticity is shown with dashed lines (see Fig. 3a for a definition of each frame). Contour lines are plotted with a spacing of 0.85 non-dimensional units. The extreme values for A_1 are ($\omega_{max} = 9.7$, $\omega_{min} = -8.2$), B_1 ($\omega_{max} = 9.5$, $\omega_{min} = -8.2$), C_1 ($\omega_{max} = 10$, $\omega_{min} = -8.2$) and A_2 ($\omega_{max} = 9.3$, $\omega_{min} = -6.5$), B_2 ($\omega_{max} = 9.03$, $\omega_{min} = -6.5$), C_2 ($\omega_{max} = 9.9$, $\omega_{min} = -6.5$).

mits a great flexibility in the plotting of I_2, p and $\dot{\omega}$.

All the isovalue contours are computed by dividing each element of the mesh into 6 or more triangles, and a linear interpolation is used over each triangle.

We present results for the two geometries described in Fig. 1a and b, respectively. The rheological contrast R_1 was taken as 1, 2.5, 5, 10 where the case $R_1 = 1$ designates the homogeneous plate model. As mentioned above, results for the rheological contrast R_2 specified in terms of the σ_y's are not different from those obtained for appropriately scaled values of R_1. For this reason, only the contour plots for $R_2 = 2.5 \times 10^3$ are discussed, the results obtained in this case are close to

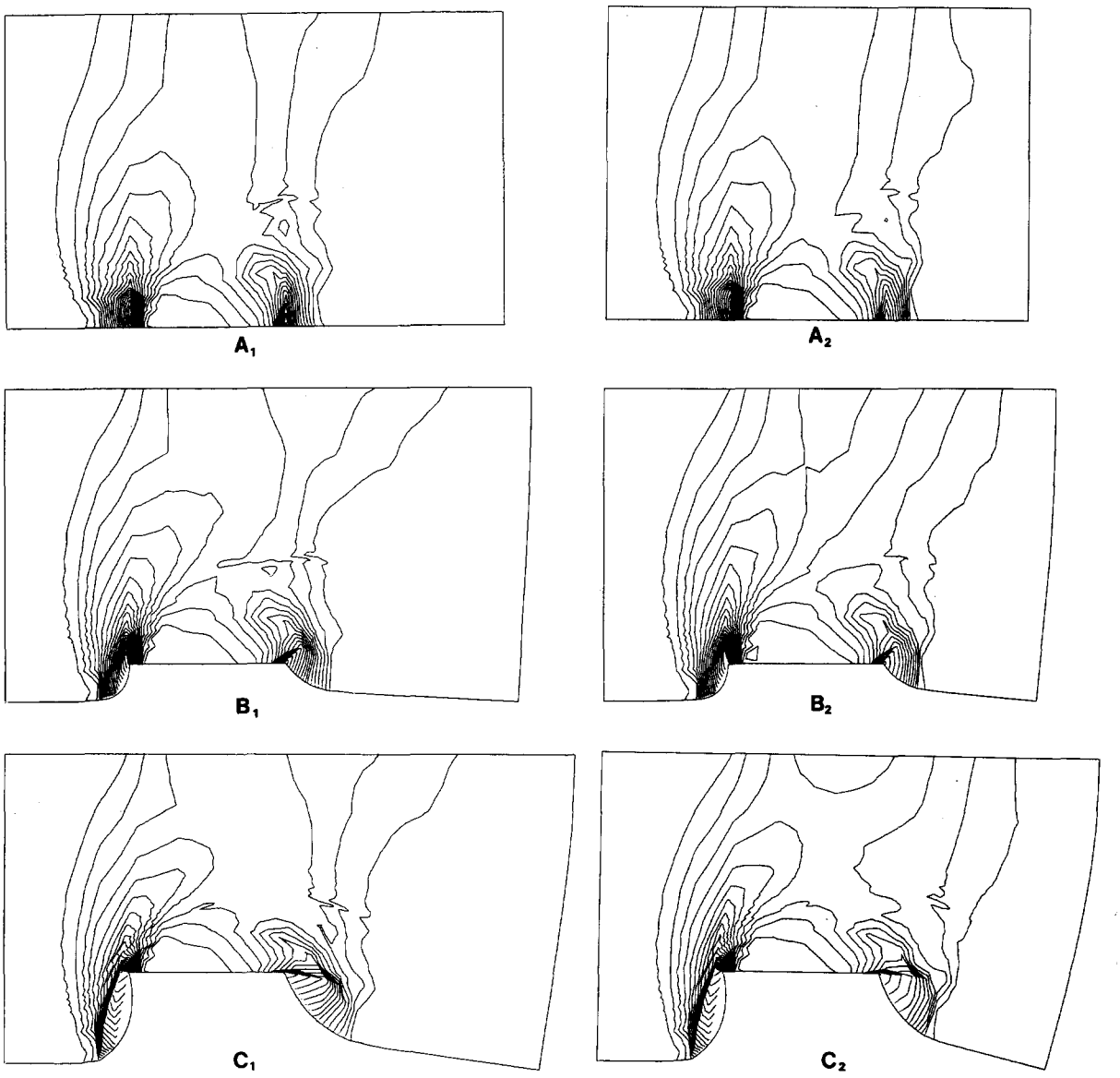

Fig. 3. (b)

those calculated for $R_1 = 5$.

We present first a detailed discussion of the results for the homogeneous case which is used as a reference for the analysis of the results for the heterogeneous models. An example of the velocity field calculated for this case, is shown on Fig. 2a, where we see that this kind of plot shows only the main features of the solution which consist in the lateral flow of material pushed by the punch. Let us discuss now the pressure, octahedral strain rate and vorticity shown in Fig. 3a, b and 3, respectively.

Contour plots at times 0, 15 and 30 Ma are shown superimposed on the updated geometry of the plate at these times.

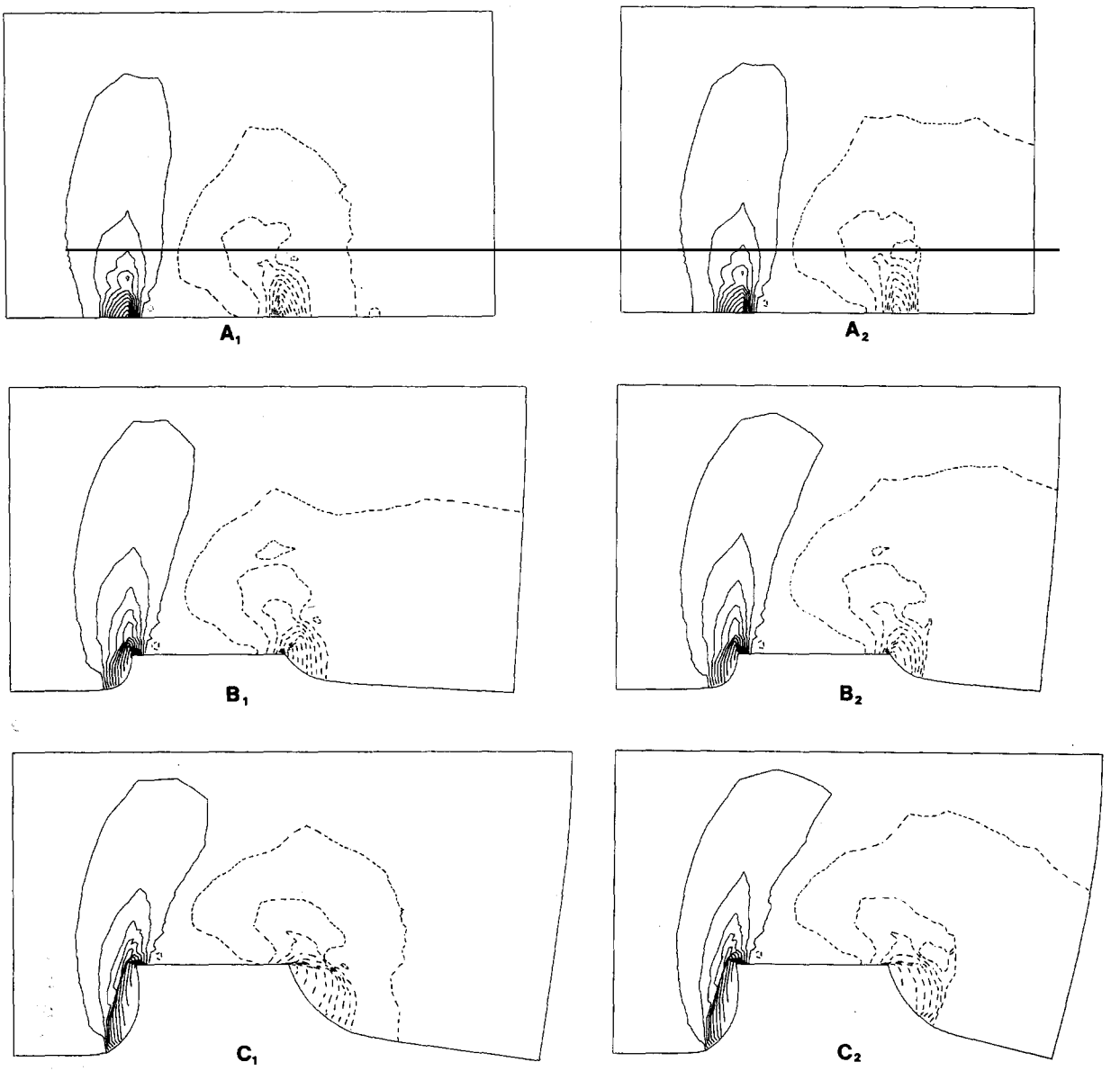

Fig. 3. (c)

4.1. Pressure (Fig. 3a)

As the penetration of the punch increases, the geometry of the pressure field changes slowly. We note first a symmetric zone in front of the indenter that tends to increase in size as it penetrates into the plate. This symmetric form defines a plateau. Near the corners of the indenter, on the other hand, we observe the development of the singularities, i.e., large concentrations of pressure and pressure gradient, that are naturally expected to form in a mixed boundary value problem. The boundary conditions on the punch are of the no-slip type, while those outside are of the free surface type. These concentrations tend to extend into the free boundaries adjacent to the punch as the deformation proceeds.

In the vicinity of the free boundaries we observe the development of negative pressure areas. These negative areas are different for the two geometries of Fig. 1a. When the BC boundary is at $1.7L$ of the punch (Fig. 1a) the negative pressure zone extends all along BC, the contour lines being parallel to the boundary. The lateral boundary plays a passive role in this case. For the initial geometry of Fig. 1b, where the boundary is at a distance L from the punch, the negative pressure zone is more restricted in area, appearing only in the lower right-hand corner of the plate. The isobars are not parallel to the boundary anymore and in fact the high pressures near the centre of the boundary are associated clearly with the sharp bend that it displays at 30 Ma (C2 in Fig. 3a). Negative pressures are associated generally with regions where there is an important change in the stress deviator which may eventually lead to its local disappearance. The close association of negative pressures with the free boundaries may also be related to the development of back arc extension, but this requires an analysis that takes into account gravitational effects.

4.2. Octahedral shear strain rate (Fig. 3b)

The octahedral shear strain rate, or second invariant of the shear strain rate tensor, is a measure of the absolute shear strain rate. Figure 3b shows that it is concentrated sharply near the edges of the indenter as a consequence of the mixed boundary condition near this edge. The strain rate concentration is larger on the left hand side of the punch, near the fixed wall AB. As the indenter penetrates, these shear zones propagate into the plate in an asymmetric way. To the left of the punch, the shear zone penetrates into the plate turning progressively to the right. This curvature of the shear zone is related closely to the presence of the fixed boundary to the north of the punch. In numerical experiments not reproduced here, we have moved this boundary further to the north. The effect of this change is to straighten the shear zones that penetrate straight into the plate, as in a snow-plow effect. Also to the left of the punch a shear zone develops behind the edge of the punch creating a sort of wake. To the right of the punch the shear zone is less developed and its curvature is in the opposite sense to that emanating from the left edge of the punch. The difference between the solutions for the initial geometries of Fig. 1a and b are small, so that we conclude that the position of the free lateral boundary does not affect the shear strain rate. The shear zone development found in our solutions is stable but it may be at the origin of instabilities leading to the development of a velocity discontinuity or fault of the type found by Tapponnier et al. (1982) in their experiments with plasticine.

4.3. Vorticity (Fig. 3c)

Vorticity is a measure of the instantaneous rate of rotation at a point in the plate. The contour lines present a clear asymmetric shape so that to the left of the punch we observe a strong localization along an elongated zone of positive vorticity (anticlockwise rotation) associated with the left-lateral shear zone that appears in the octahedral shear strain rate. To the right of the punch the contours are more spread and indicate negative (right lateral) rotation rate. The free boundary conditions to the right of the punch appear to control the vorticity distribution because a roughly rectangular block at the bottom left of the plate rotates counterclockwise with an almost rigid motion. The rotation of this block increases as the lateral boundary approaches the punch. Similar

observations were made by Tapponnier et al. (1982) for their plasticine experiments. The sharp bend of the right hand side of the plate in the case of the shorter plate is clearly associated with the quasi-rigid rotation of the block at the bottom right of the plate.

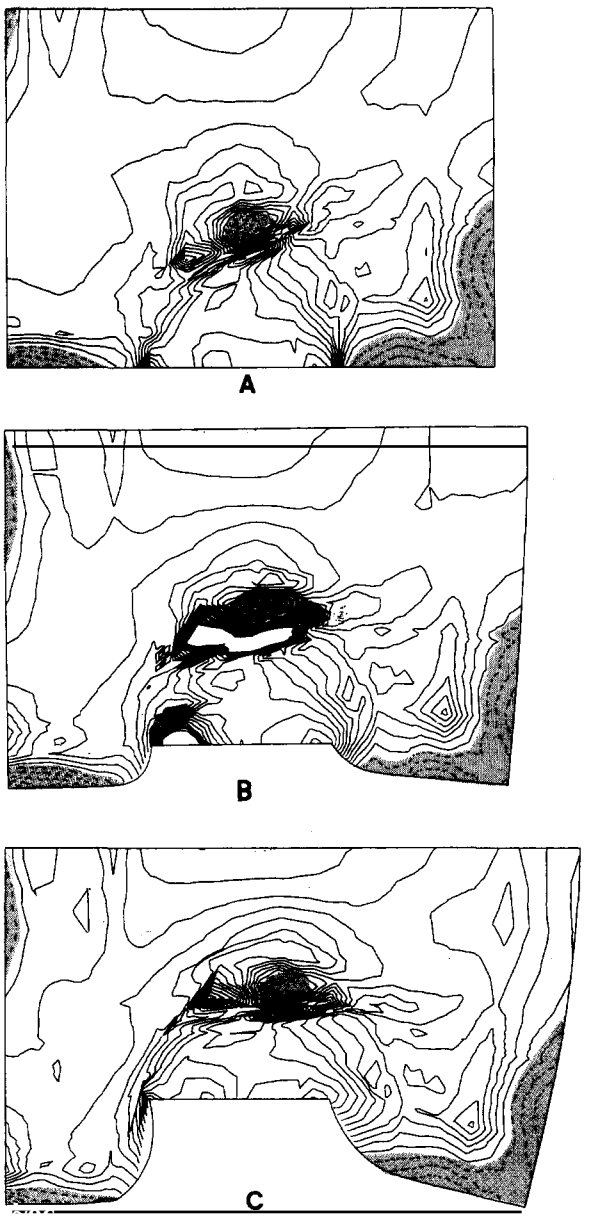

5. Results for a heterogeneous plate

In this section, we discuss the results obtained for a heterogeneous plate containing an inclusion of the shape shown in Fig. 1. The effects of the inclusion on the flow field are extremely important even for small contrasts of rheological properties. The main effect that will be discussed is the development of sharp shear zones in front of the heterogeneities. Figure 2b shows again an example of the velocity field obtained for a particular realisation of the numerical experiment. It is difficult to determine from an analysis of Fig. 2a and b what are the main effects of the presence of a heterogeneous zone. This is the reason why we prefer to discuss

Fig. 4.(a) Pressure field for the heterogeneous plate model ($R_2 = 2.5 \times 10^2$) with the initial geometry shown in Fig. 1c. A, B, C are calculated at 1, 15 and 30 Ma, respectively. Negative pressure areas are shaded. Contour lines are plotted with a spacing of 0.62 non-dimensional units. Extreme values of A are ($P_{max} = 7.3$, $P_{min} = -4.4$), B ($P_{max} = 11.4$, $P_{min} = -6.9$), C ($P_{max} = 8.07$, $P_{min} = -4.4$). (b) Pressure field for the heterogeneous plate model ($R_1 = 2.5$) of initial geometry shown in Fig. 1a, b. The frames are defined in Fig. 3a. Negative pressure areas are shaded. Contour lines are plotted with a spacing 1.1 non-dimensional units. Extreme values are A_1 ($P_{max} = 15.6$, $P_{min} = -7.71$), B_1 ($P_{max} = 16$, $P_{min} = -7.71$), C_1 ($P_{max} = 16.4$, $P_{min} = -5.5$) and A_2 ($P_{max} = 15.4$, $P_{min} = -8.8$), B_2 ($P_{max} = 15.6$, $P_{min} = -8.8$), C_2 ($P_{max} = 16.6$, $P_{min} = -8.8$). (c) Pressure field for the heterogeneous plate model ($R_1 = 5.0$) of initial geometry shown in Fig. 1a, b. The frames are defined in Fig. 3a. Negative pressure areas are shaded. Contour lines are plotted with a spacing of 1.34 non-dimensional units. Extreme values are A_1 ($P_{max} = 17.1$, $P_{min} = -8.2$), B_1 ($P_{max} = 16.8$, $P_{min} = -8.2$), C_1 ($P_{max} = 17.6$, $P_{min} = -9.5$) and A_2 ($P_{max} = 16.7$, $P_{min} = -8.2$, B_2 ($P_{max} = 16.5$, $P_{min} = -9.5$), C_2 ($P_{max} = 22.8$, $P_{min} = -9.5$). (d) Pressure field for the heterogeneous plate model ($R_1 = 10$) with the initial geometry of Fig. 1a, b. The frames are defined in Fig. 3a. Negative pressure areas are shaded. Contour lines are plotted with a spacing of 2 non-dimensional units. Extreme values are A_1 ($P_{max} = 40.5$, $P_{min} = -14.6$), B_1 ($P_{max} = 39.9$, $P_{min} = -17.4$), C_1 ($P_{max} = 39.8$, $P_{min} = -17.4$) and A_2 ($P_{max} = 39.7$, $P_{min} = -17.4$), B_2 ($P_{max} = 38.6$, $P_{min} = -17.4$), C_2 ($P_{max} = 38.0$, $P_{min} = -17.4$). (e) Pressure field for the heterogeneous plate model ($R_2 = 2.5 \times 10^2$) with the initial geometry of Fig. 1a, b. The frames are defined in Fig. 3a. Negative pressure areas are shaded. Contour lines are plotted with a spacing of 0.45 non-dimensional units. Extreme values are A ($P_{max} = 5.7$, $P_{min} = -3.07$), B ($P_{max} = 13.7$, $P_{min} = -5.77$), C ($P_{max} = 6.4$, $P_{min} = -3.07$).

our results on the basis of the contour plots of pressure, shear strain rate and vorticity.

5.1. Pressure (Fig. 4a, b, c, d, e)

The pressure field is affected drastically by the presence of the heterogeneity as a comparison with Fig. 3b will readily show. We notice a negative pressure region that develops above and in the immediate neighbourhood of the heterogeneity. The size of this zone and its amplitude are controlled naturally by the size of the heterogeneity and its contrast. We present the result for five numerical experiments: Fig. 4a is the pressure field for the small heterogeneity narrower than the size of the punch shown in Fig. 1c; Fig. 4b, c and d are

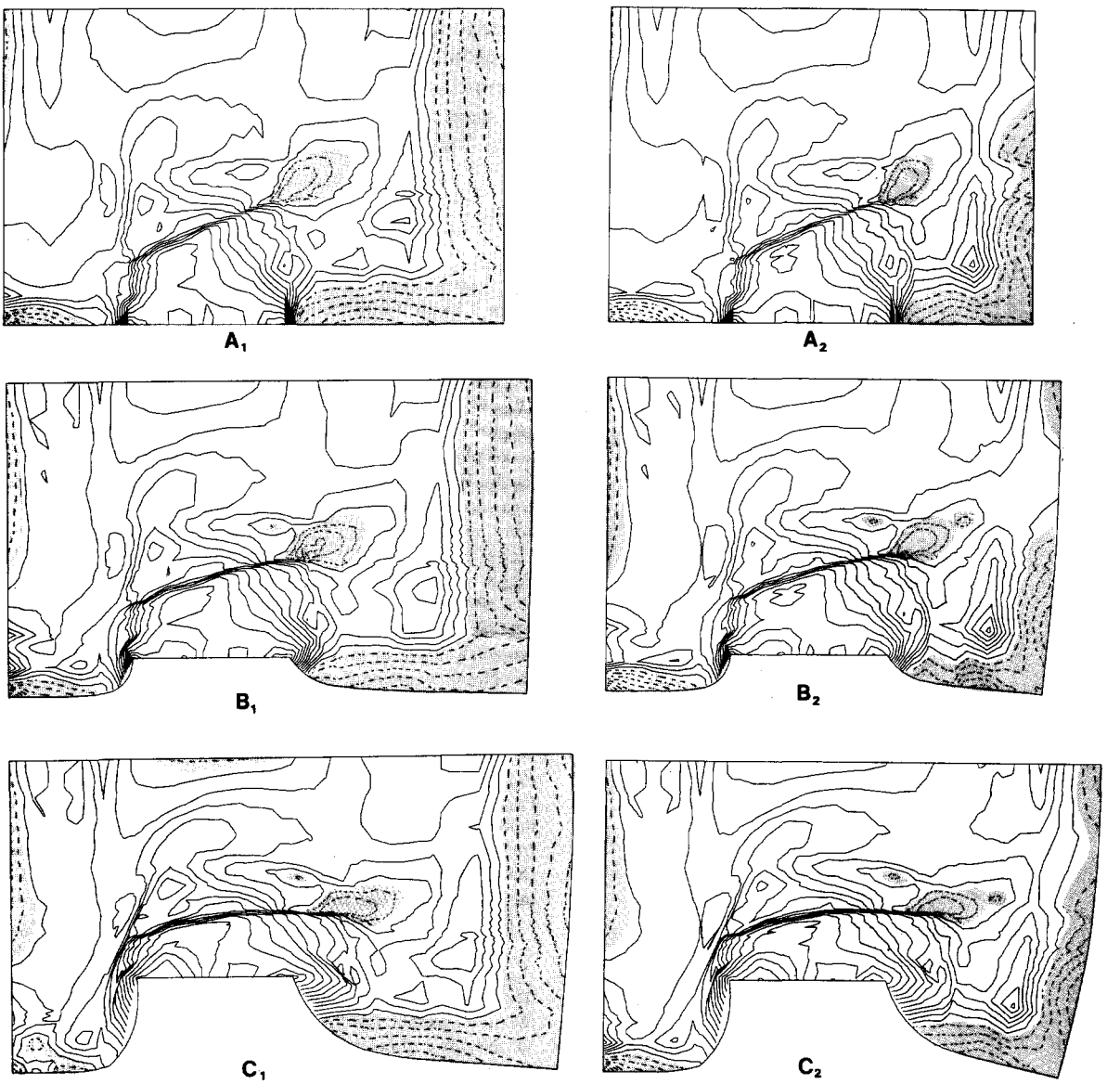

Fig. 4. (b)

the results for the heterogeneity of Fig. 1 for three different contrasts of yield stress i.e., $R_1 = 2.5$, 5 and 10, respectively. In this way we can appreciate the effect of increasing the the rigidity of the heterogeneity. Finally, Fig. 4e shows the results for a case in which we change the creep fluidity γ of the heterogeneity while σ_y does not change. In this example, $R_2 = 2.5 \times 10^3$. The results for this experiment are not very different from those of Fig. 4c for the case $R_1 = 5$. Similarly, the results of Fig.

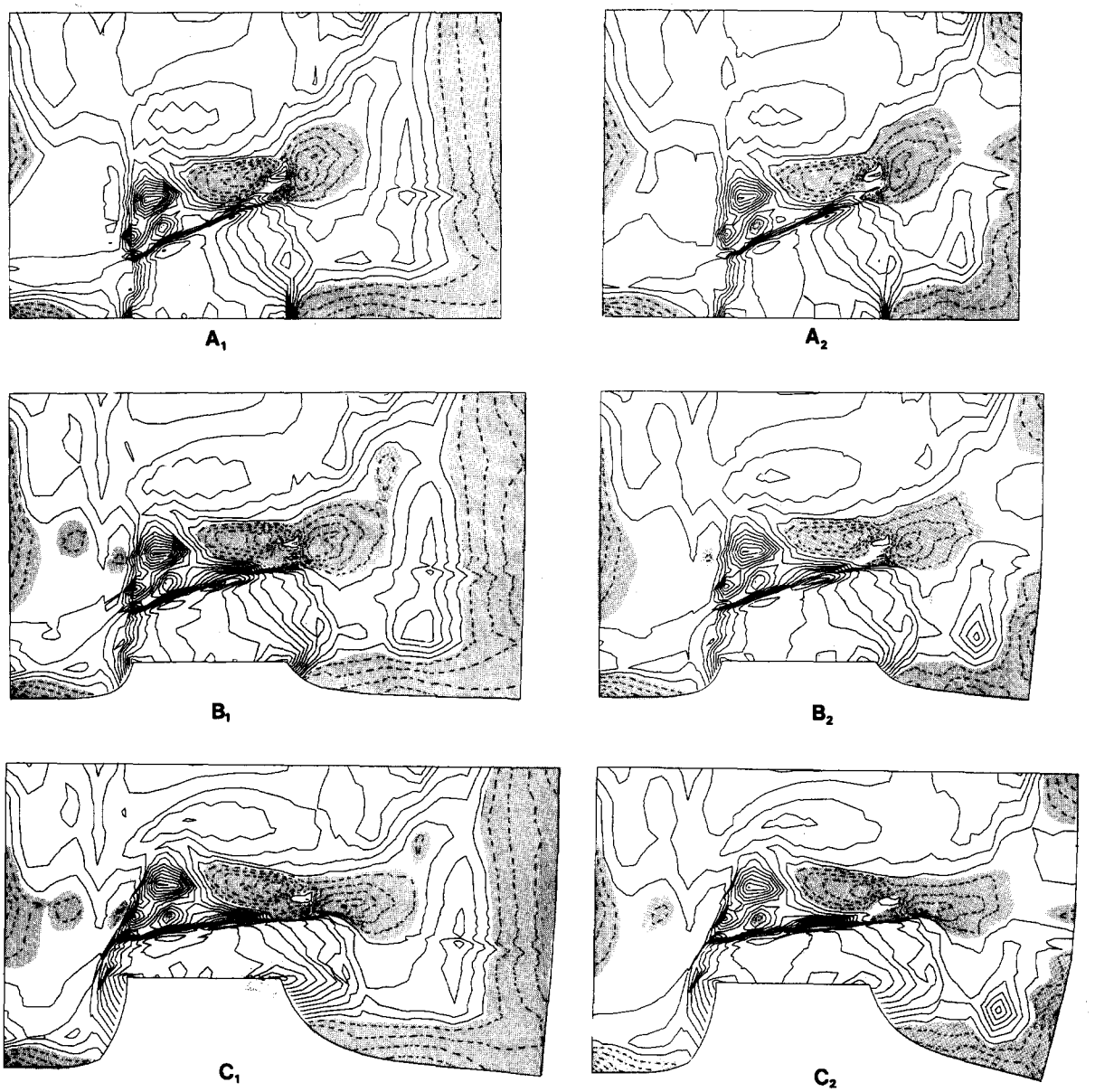

Fig. 4. (c)

4d are close to those of Fig. 4c. For the strain rate and vorticity fields only the fields corresponding to 4a, b and c are presented.

In the case of a small scale heterogeneity (Fig. 4a) a negative pressure zone develops above the inclusion behind a narrow zone of high positive pressures. For the larger scale heterogeneity the negative pressure area increases in size with increasing rheological contrast. In Fig. 4b, where $R_1 = 2.5$, the negative pressure appears only behind the right tip of the elongated positive pressure anomaly. Thus, the leading edge of the inclusion develops a large linear concentration of pressure, shear strain and vorticity. This shear zone would develop into a fault if we had included a strain softening mechanism in the plastic rheology.

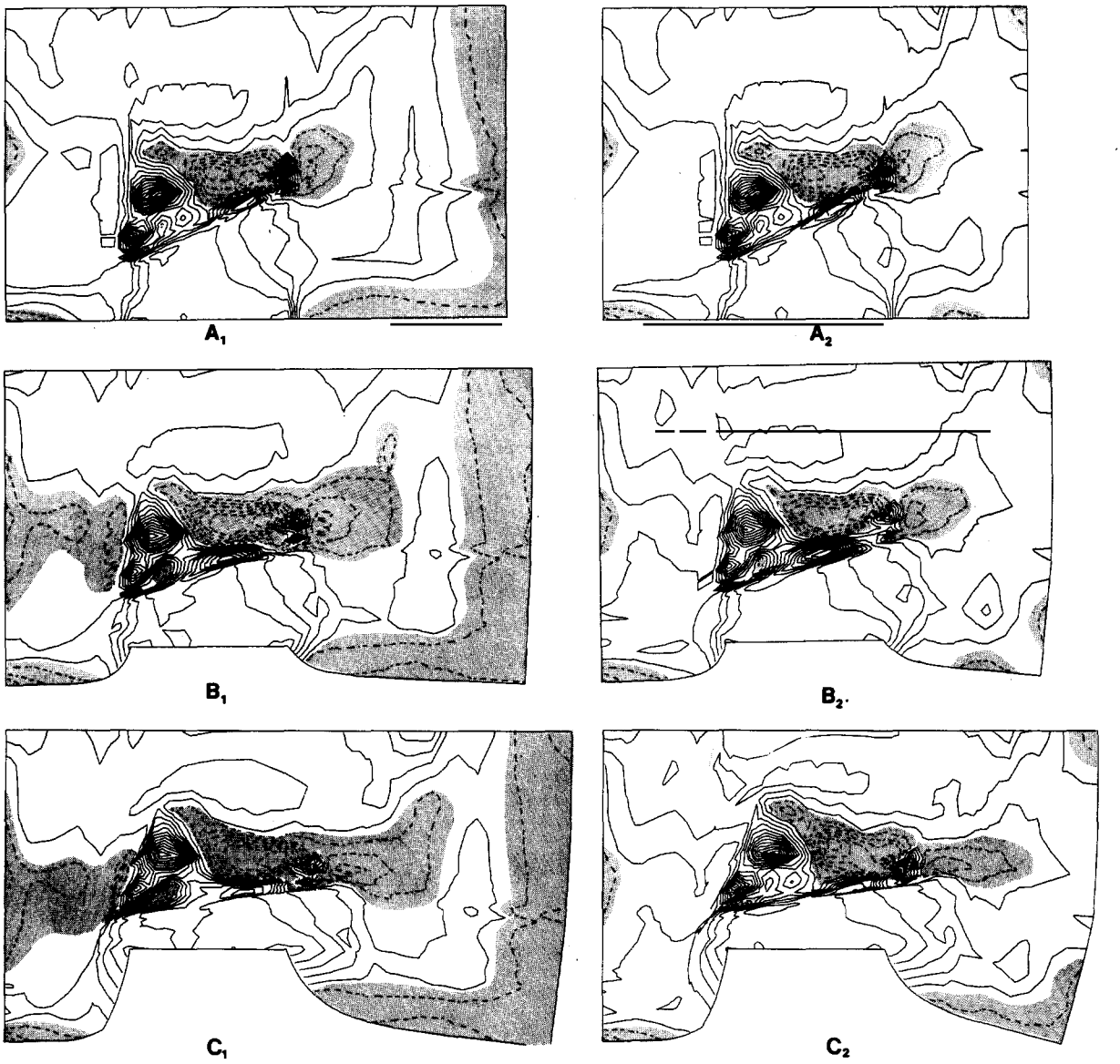

Fig. 4. (d)

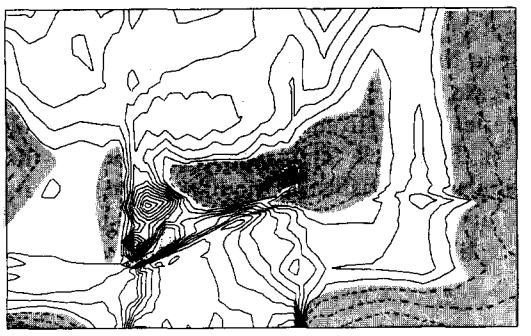

A

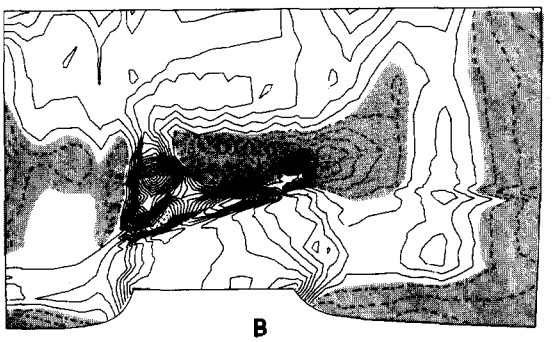

B

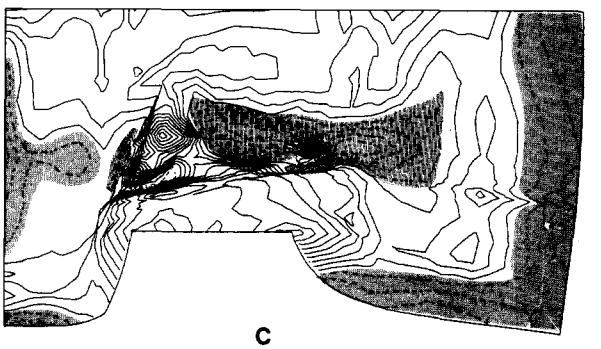

C

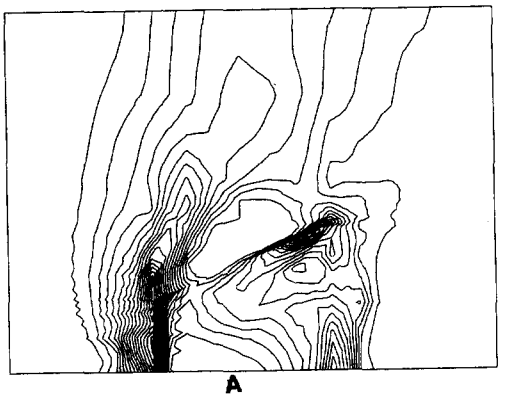

A

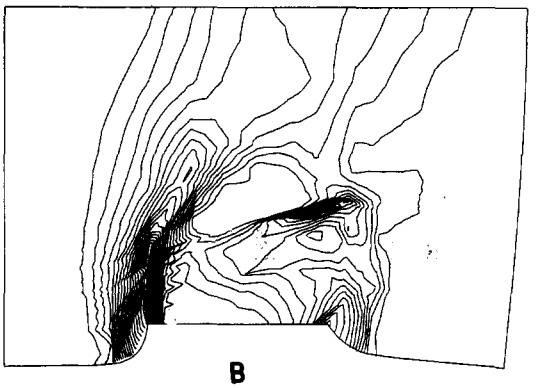

B

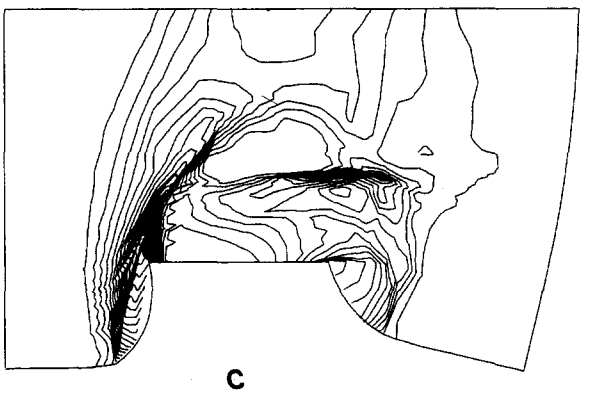

C

Fig. 5. (a) Octahedral shear strain rates for the heterogeneous plate model ($R_2 = 2.5\times10^2$) of initial geometry as shown in Fig. 1c. The frames A, B, C are for times 0, 15 and 30 Ma, respectively. Contour lines are plotted with a spacing of 0.36 non-dimensional units. Extreme values are A ($I_{2_{max}} = 7.0$, $I_{2_{min}} = 0.11\times10^{-4}$), B ($I_{2_{max}} = 7.6$, $I_{2_{min}} = 0.11\times10^{-4}$), C ($I_{2_{max}} = 7.15$, $I_{2_{min}} = 0.11\times10^{-4}$). (b) Octahedral shear strain rates for the heterogeneous plate model ($R_1 = 2.5$) of initial geometry as shown in Fig. 1a, b. The frames are defined in Fig. 3a. Contour lines are plotted with a spacing of 0.52 non dimensional units. Extreme values are A_1 ($I_{2_{max}} = 8.02$, $I_{2_{min}} = 0.8\times10^{-4}$), B_1 ($I_{2_{max}} = 9.8$, $I_{2_{min}} = 0.8\times10^{-4}$), C_1 ($I_{2_{max}} = 9.0$, $I_{2_{min}} = 0.8\times10^{-4}$) and A_2 ($I_{2_{max}} = 9.0$, $I_{2_{min}} = 8\times10^{-4}$), B_2 ($I_{2_{max}} = 10.6$, $I_{2_{min}} = 0.8\times10^{-4}$), C_2 ($I_{2_{max}} = 10.2$, $I_{2_{min}} = 0.8\times10^{-4}$). (c) Octahedral shear strain rates for the heterogeneous plate model ($R_1 = 5.0$) for the initial geometry shown in Fig. 1 a, b. The frames are defined in Fig. 3a. Contour lines are plotted with a spacing of 0.65 non-dimensional units. Extreme values are A_1 ($I_{2_{max}} = 11.9$, $I_{2_{min}} = 0.7\times10^{-5}$), B_1 ($I_{2_{max}} = 13.04$. $I_{2_{min}} = 0.7\times10^{-5}$), C_1 ($I_{2_{max}} = 13.1$, $I_{2_{min}} = 0.7\times10^{-5}$) and A_2 ($I_{2_{max}} = 11.2$, $I_{2_{min}} = 0.7\times10^{-5}$), B_2 ($I_{2_{max}} = 12.23$, $I_{2_{min}} = 0.7\times10^{-5}$), C_2 ($I_{2_{max}} = 12.0$, $I_{2_{min}} = 0.7\times10^{-5}$).

For the temperature independent exponential creep law used in this study, the shear zone remains stable. As the rheology contrast increases (Fig. 4c and d) the negative pressure zone increases also in size, eventually becoming slightly larger in area than the inclusion. For $R_1 = 5$ and 10 a negative pressure zone develops to the left of the inclusion. The rotation of the inclusion as it is pushed by the punch creates a suction on the fixed boundary. The rest of the features of the pressure fields are similar to those already discussed for the homogeneous case, i.e., negative pressures near the free boundaries and strong concentrations near the edges of the punch. Thus, the main effect of the inclusion is to drastically modify the field in its immediate vicinity creating a high pressure ridge in its leading edge and negative pressures on its surface.

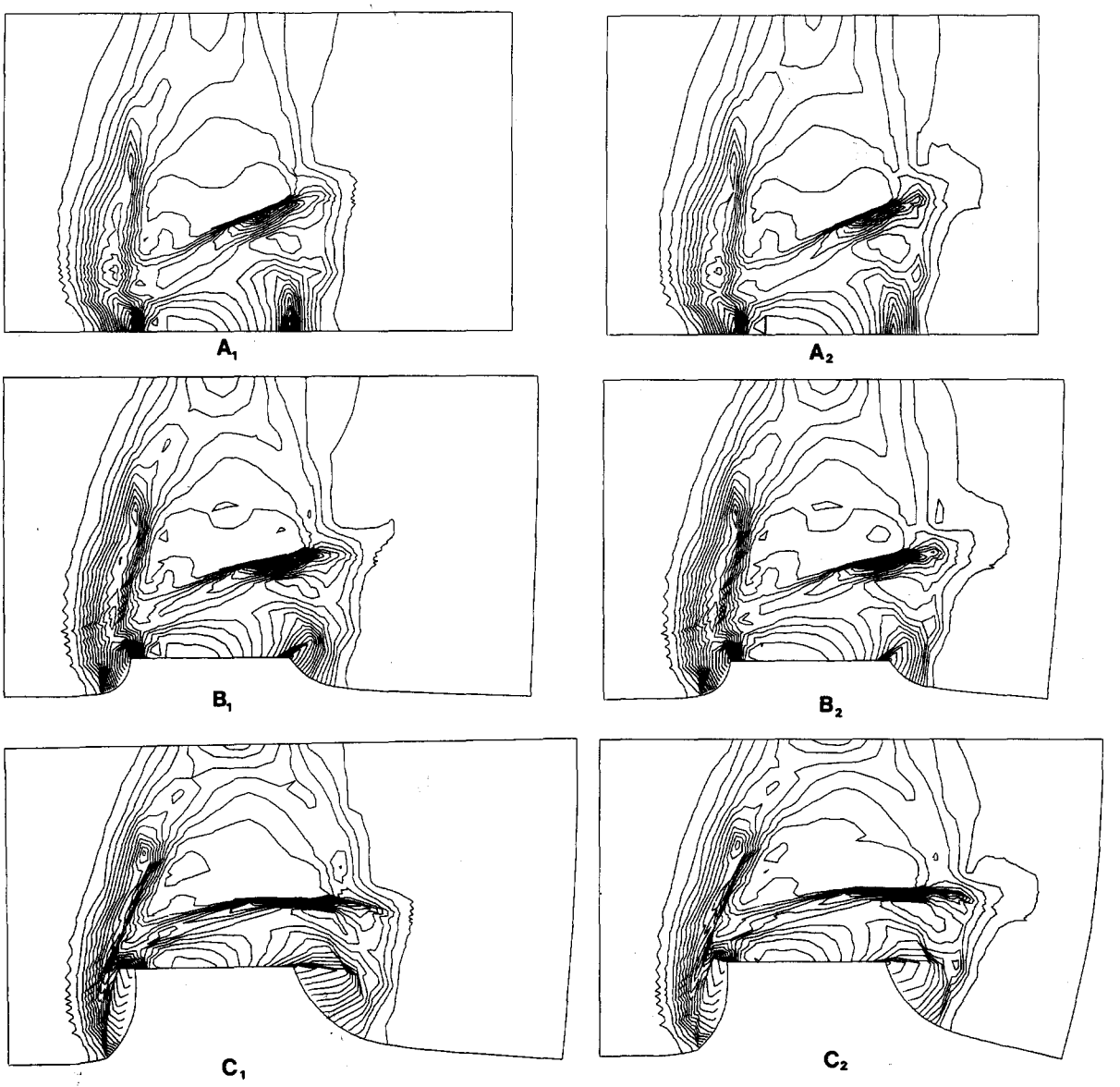

Fig. 5. (b)

5.2. Octahedral shear strain rate (Fig. 5a, b, c)

The presence of the heterogeneity creates two zones of strong shear concentration. The first one is at the leading edge of the inclusion, the other one at the left hand side of it. The frontal shear zone develops progressively and presents a maximum shear concentration near its right end. As the indention proceeds, it tends to bend and become parallel to the punch front. This is due to a strong clockwise rotation of the inclusion. As the rigidity contrast increases (cf. Fig. 5b and c) the shear zone becomes narrower and shear strain rate increases. Comparing with the results for the pres-

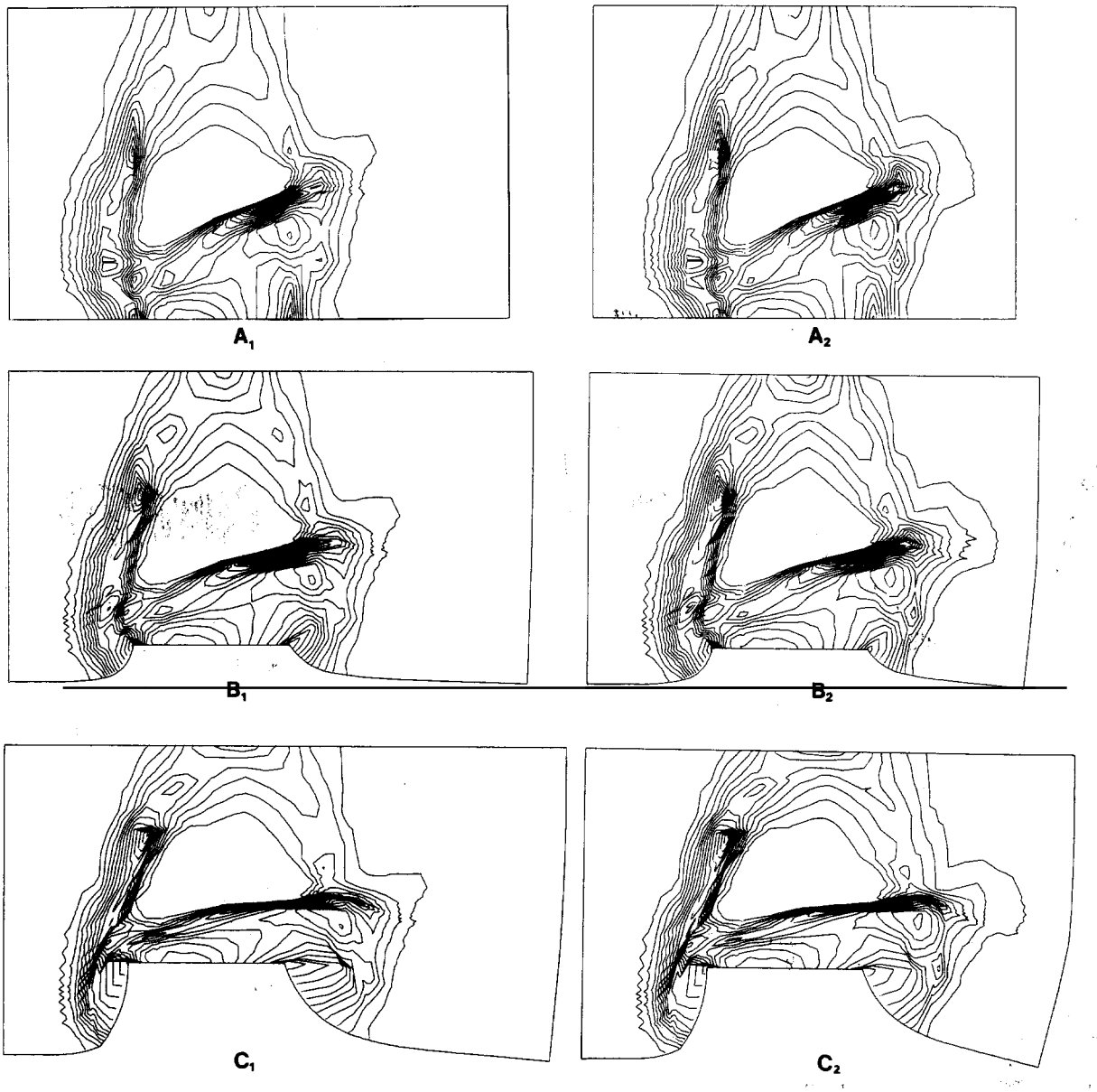

Fig. 5. (c)

sure field shown in Fig. 4b and c one sees that the narrowing of the shear zone and the development of the negative pressure zone on the inclusion go hand in hand.

The second shear zone, to the left of the inclusion, has a geometry that changes with the rheology contrast and the size of the heterogeneity. For the small inclusion, Fig. 5a, the shear zone bends sharply to the right and tends to develop behind the heterogeneity, i.e., the flow tends to create conditions of free slip around the heterogeneity that becomes a rigid particle carried by the flow. For the larger inclusions (Fig. 5b and c) the curvature of the shear zone increases with the rheological contrast R_1. As for the homogeneous case the position of the lateral boundary is not important for the shear strain field.

5.3. Vorticity (Fig. 6a, b, c)

The shear zones described above are also clearly marked in the vorticity maps with two vortex sheets that coincide with the shear zones. Along the lower boundary of the inclusion a positive (counterclockwise) rotation is localized and develops progressively as the indenter penetrates into the plate. This sense of rotation is coherent with a left lateral motion along the boundary of the heterogeneity.

To the left of the inclusion, there is another elongated high vorticity zone which becomes narrower and more bent to the right as the heterogeneous block rotates clockwise under the pressure from the punch. For the larger value of $R_1 = 5$, Fig. 6c, the left-hand side zone separates into two areas of high vorticity. One associated with the left-hand boundary of the block where left lateral (positive) rotation occurs and another zone trailing

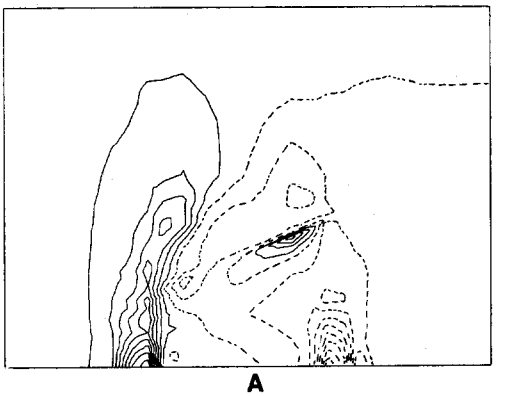

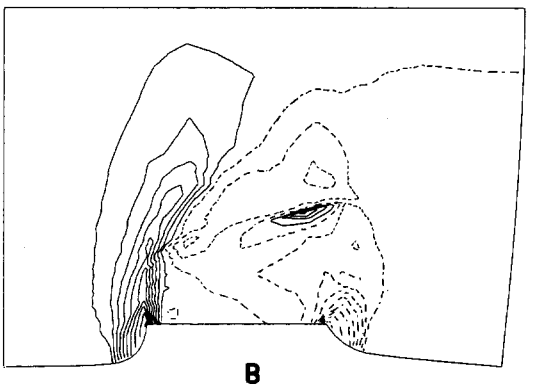

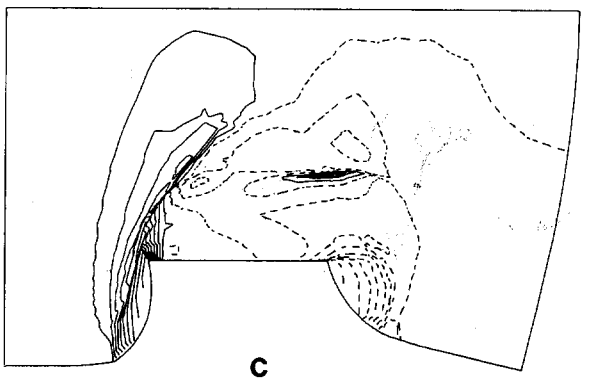

Fig. 6. (a) Vorticity for the heterogeneous plate model ($R_2 = 2.5 \times 10^2$) with the initial geometry shown in Fig. 1c. Dashed lines indicate negative vorticity. A, B, C for 0, 15, 30 Ma. Contour lines are plotted with a spacing of 1.0 non dimensional units. Extreme values are A ($\omega_{max} = 8.7$, $\omega_{min} = -10.2$), B ($\omega_{max} = 9.0$, $\omega_{min} = -12$), C ($\omega_{max} = 9.8$, $\omega_{min} = -10.2$). (b) Vorticity for the heterogeneous plate model ($R_1 = 2.5$) with the initial geometry shown in Fig. 1 a, b. The frames are defined in Fig. 3a. Dashed lines indicate negative vorticity. Contour lines are plotted with a spacing of 1.1 non dimensional units. Extreme values are A_1 ($\omega_{max} = 9.4$, $\omega_{min} = -9.6$), B_1 ($\omega_{max} = 9.8$, $\omega_{min} = -10.7$), C_1 ($\omega_{max} = 10.9$, $\omega_{min} = -10.7$) and A_2 ($\omega_{max} = 8.3$, $\omega_{min} = -8.5$), B_2 ($\omega_{max} = 8.90$, $\omega_{min} = -8.5$), C_2 ($\omega_{max} = 9.6$, $\omega_{min} = -9.6$). (c) Vorticity of the heterogeneous plate model ($R_1 = 5.0$) for the initial geometry shown in Fig. 1a, b. The frames are defined in Fig. 3a. Dashed contours indicate negative vorticity. Contour lines are plotted with a spacing of 1.0 non dimensional units. Extreme values are A_1 ($\omega_{max} = 9.05$, $\omega_{min} = -10.4$), B_1 ($\omega_{max} = 9.8$, $\omega_{min} = -10.4$), C_1 ($\omega_{max} = 9.1$, $\omega_{min} = -8.4$), C_2 ($\omega_{max} = 9.1$, $\omega_{min} = -8.4$).

behind the left hand edge of the punch. Two zones of negative vorticity also are clearly distinguished, one associated with the clockwise rotation of the heterogeneity, the other with the lower right hand corner of the plate which produces the sharp bend of the right-hand boundary of the plate in the case $R_1 = 5$. As the right-hand boundary of the plate gets closer to the punch the rotation of the lower right hand corner increases.

5.4. *Finite deformation*

Our numerical technique allows for an integration of the strain rates as the deformation pro-

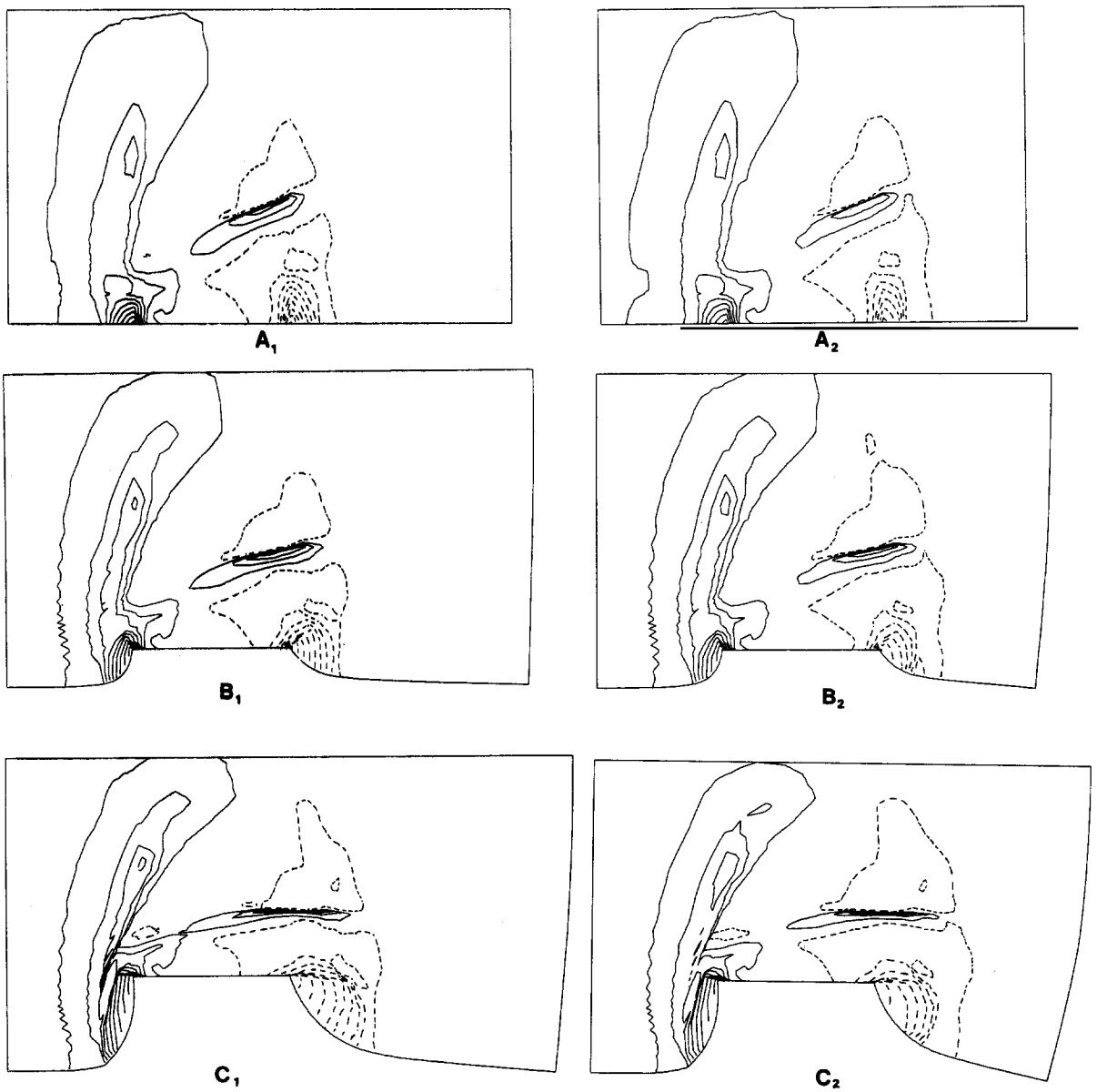

Fig. 6. (b)

ceeds. In this way we can recalculate the shape of the plate as a function of time and obtain its finite deformation. In Fig. 7 we present the deformation of the borders of the plate and of the heterogeneity as a function of time for four different contrasts of rigidity $R_1 = 1$ (homogeneous), $R_1 = 2.5$, 5 and 10.

The finite rotation of the block as a function of time appears clearly in these figures, as well as its internal deformation into a dog bone shape. As R increases we observe that the inclusion becomes more and more undeformable and rotates as a rigid body. Also, it is interesting to note that the

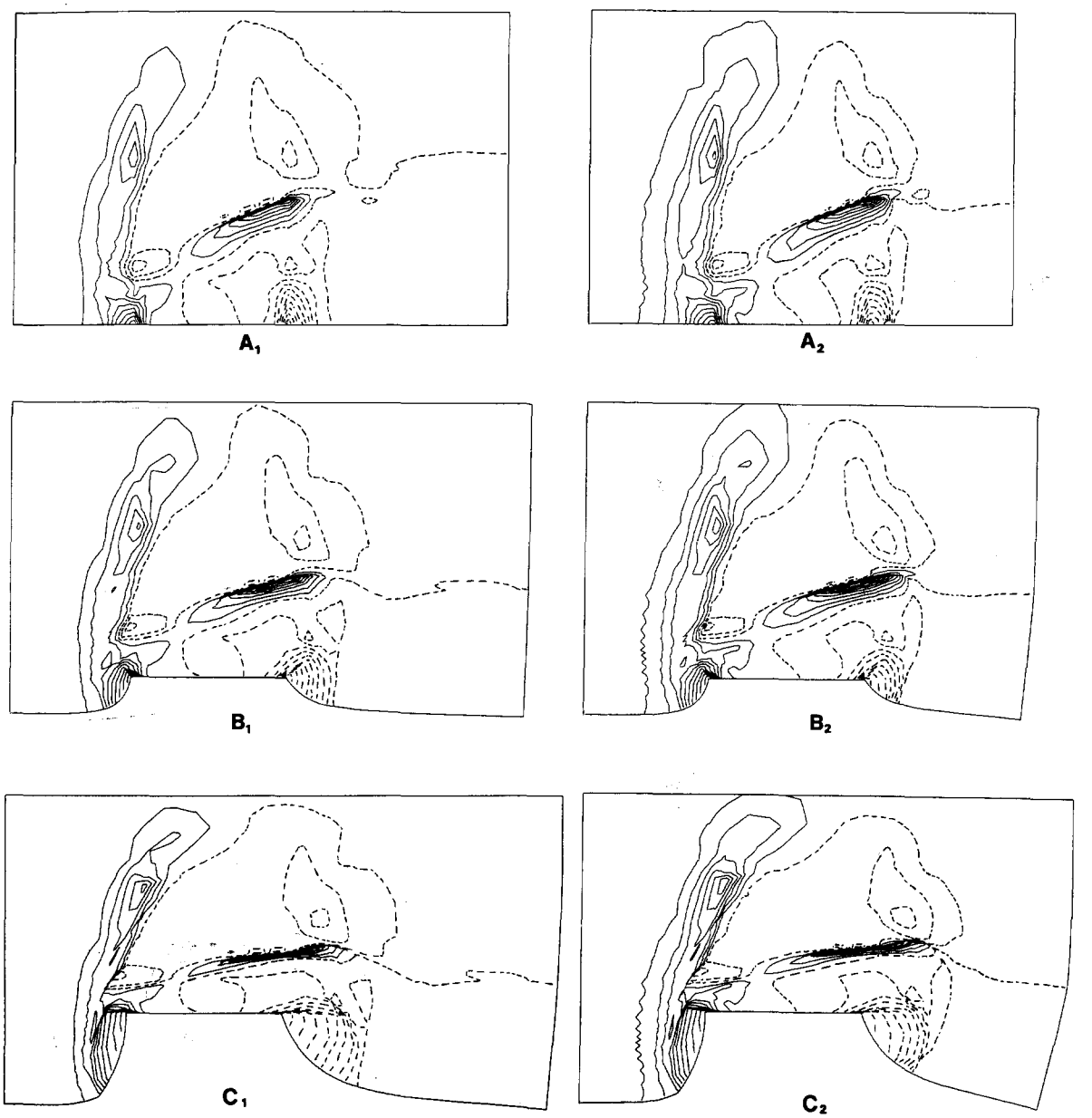

Fig. 6. (c)

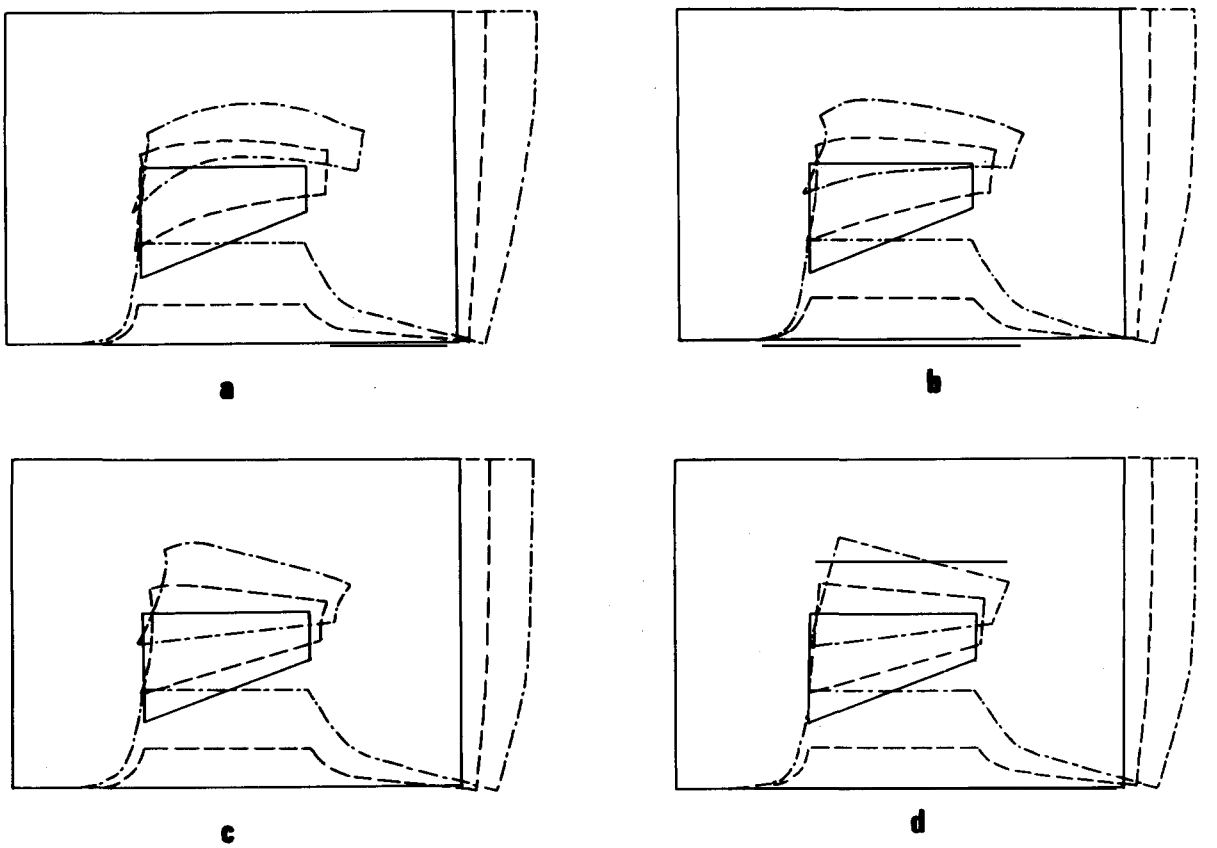

Fig. 7. Finite deformation of the shape of the plate and the inclusion as a function of time. The initial model is that of Fig. 1b. The position and shape are shown with full line for $t = 0$, dashed line for $t = 15$ Ma, dot-dashed line for $t = 30$ Ma. Each frame is for a different rigidity contrast R_1: (a) $R_1 = 1$, (b) $R_1 = 2.5$, (c) $R_1 = 5$ and (d) $R_1 = 10$.

bend of the righthand side of the plate increases with increasing R_1.

Discussion

We have presented the results of a study of the finite deformation of a viscoplastic plate indented by a rigid punch. Both a homogeneous plate model and another one containing a heterogeneous inclusion were analyzed assuming a plane strain mode of deformation. According to a previous study (Vilotte et al., 1982) the results for plane stress should not differ much from those found here as long as free boundary conditions are imposed on the lefthand side of the plate. The numerical technique is an improvement on that used by Vilotte et al. (1982) because we may now determine finite deformation by means of a time integration of the particle velocities of the finite element grid. This allows us to calculate on the updated geometry of the initially rectangular plate for times of up to 30 Ma. We have assumed a viscoplastic behaviour combining a yield stress and a power law creep rheology for the depth-averaged properties of the lithosphere. Our numerical technique assumes a continuous deformation field, so that we do not allow for the formation of internal slip discontinuities or faults. We may interpret, however the shear zones developed near the heterogeneity as the initial stages of the formation of faults. In the interpretation of results it may be assumed that these narrow shear zones would eventually develop into faults if a fracture mechanism was included in the rheology.

The interpretation of the pressure field also

requires some clarification. The zones where large positive pressures develop may be interpreted as areas where the plane strain approximation is inadequate, since for a finite depth plate these areas would naturally tend to thicken. The negative pressure areas are more delicate to interpret: Tapponnier (1978) proposed that these areas would tend to get thinner, and may eventually become the site of active extensional tectonics. The detailed analysis of such zones requires the introduction of buoyancy forces which may sometimes modify this simple interpretation (Vilotte et al. 1984). For the purposes of the present discussion, where buoyancy forces are absent, we assume a perfect correlation between high and low pressure areas in plane strain and thick and thin areas in plane stress.

Most of the results obtained for the homogeneous plate model are similar to those of Vilotte et al. (1982) for the initial stages of the flow ($t < 5$ Ma), where the deformation of the plate does not affect the strain velocity and stress fields. The progressive development of the shear zones in Fig. 3b may be naturally related to the existence in the Asian plate of 2 families of strike slip faults (Tapponnier and Molnar, 1976). The asymmetric development of the shear zones with a much stronger one originating at the left hand edge of the punch may also be related to observations in Asia since this shear zone tends to bend clockwise in the direction of the free lateral boundary. This may explain the curved shape of the great strike slip faults of western China which have frequently been related to the geometry of the slip lines for the perfectly plastic model of the punch (Molnar and Tapponnier, 1976). We believe, however, that the curved shape of the shear zones is controlled closely by the geometry of the plate and the boundary conditions. When the northern boundary of the plate is moved further away from the punch, the curvature of the strain concentrations tends to disappear and the punch penetrates more like a snow plow along two straight shear zones perpendicular to the punch front. If this model is applicable to Asia, then the curvature of the great strike slip fault of China may be controlled by the presence of the rigid Siberian platform and the free boundary conditions at the West Pacific subduction zones. The strong shear strain concentration on the wake of the punch to its left may be also related to certain features observed in Asia, like the Quetta–Chaman fault.

The presence of an inhomogeneous zone perturbs in a fundamental way the homogeneous solutions even for small rheological contrasts and sizes of the heterogeneity. This is due to the highly non linear nature of the viscoplastic flow. We may roughly describe the inclusion as a slightly deformable raft drifting in the viscoplastic flow of the surrounding plate. A clear shear zone appears in front (the leading edge) of the inclusion which delineates the transition between the main plastic flow in the plate and the inhomogeneity. This is a sort of internal boundary layer with strong concentration of positive pressure (tendency to thicken the plate), high shear strain rates and right lateral (negative) vorticity. The inclusion becomes progressively detached from the main flow and eventually, if slip discontinuities were allowed in our model, a fault zone would develop along this boundary. The geometry and the direction of shear along this boundary layer is similar to that of the Altyn Tagh fault that separates the Tarim basin from Tibet. In fact, the geometry of our inclusion (described in Fig. 1) was chosen so that it roughly approximates the position and shape of the Tarim basin with respect to the Himalayan thrust. The geometry and the amount of localization (narrowness) of the shear zone depends directly on the rheological contrast between the plate and the inclusion, but it is present even for small rheological contrast and small size heterogeneities. It appears to be a stable feature of flow around inhomogeneous inclusions. For a small rheological contrast $R_1 = 2.5$, the negative pressure zone behind the shear zone is localized near its right end. These negative pressures appear always near the tip of faults or the ends of narrow shear zones. If we accept that the negative pressures are associated with a thinning of the lithosphere, these negative pressure zones may be associated with the Shansi in Asia. For greater rheological contrasts ($R_1 = 5$ or 10) the negative pressure zone grows, eventually becoming larger in surface than the heterogeneity itself. This result is in good agreement with the depressed nature of the Tarim and its northern end (Molnar and Tapponnier, 1981), but it certainly deserves reexamination taking buoyancy forces into account.

The rotation and lateral motion of the inclu-

sion, as shown in Fig. 7, is also closely related to an important rotation of the lower right compartment of the plate, which tends to get decoupled from the rest of the plate. The strong bending of the lateral boundary near its centre reflects this rotation. As R_1 increases, the rotation increases and the decoupling of this corner becomes more effective as observed in the progressive bending of the lateral boundary. For a plate model that incorporates a rupture mechanism we would expect that eventually a fault would propagate from the end of the shear zone in front of the inclusion, to the lateral boundary. This is what is observed in the plasticine models studied by Tapponnier et al., 1982, who also noticed that the rotation of this block is related to a rotation of Indo-China. Note however, that in our numerical models the rotation of the lower right hand corner is related to the presence of a heterogeneity. Its rotation in the case of the homogeneous plate model is small and we could hardly expect the development of a fault like F_1 in the Tapponnier et al. (1982) experiment.

Further analysis of the geophysical applications of this model would require additional data on the rotation of the Tarim block, for instance palaeomagnetic directions, which are not available at present. The goal of our study was to establish some simple properties of the flow around the inhomogeneity that could be used to analyze geophysical examples, and to determine the main kinematical features of the flow. The most important result is that strong shear zones or internal boundary layers develop in front and to the left of the heterogeneity, tending to decouple it from the viscoplastic flow in the plate. The fact that this mechanism develops for small and large heterogeneities underlines the importance of inclusions in the flow of the lithosphere. It also opens certain questions about the way we can homogenize or average the plastic behaviour of the lithosphere over large areas; in particular, what are the mean plastic properties of a plate segment that contains inclusions of variable rigidity at all scales?

Acknowledgements

J.P. Vilotte has been supported at The University College of Swansea by a fellowship of the Royal Society. This research was funded by grants from the ATP Geodynamique II of the Institute National d'Astronomie et Geophysique in France. IPG publication No.

References

Caby, R., Bertrand, J.M. and Black, R., 1981. Pan-African ocean closure and continental collision in the Hoggar–Iforas segment, Central Sahara. In: A. Kröner (Editor), Precambrian Plate Tectonics. Elsevier, Amsterdam, pp. 407–434.

Daignieres, M., Fremond, M. and Friaa, A., 1978. Modèle de type Norton-Hoff généralisé pour l'étude des déformations lithosphériques (exemple: la collision Himalayenne). C. R. Acad. Sci. Paris, 268, B: 371–374.

England, P. and McKenzie, D.P., 1982. A thin viscous sheet model for continental deformation. Geophys. J.R. Soc., 70: 295–322.

England, P. and McKenzie, D.P., 1983. Correction to a thin viscous sheet model for continental deformation. Geophys. J.R. Astron. Soc., 73: 523–532.

Mandel, J., 1971. Plasticité classique et viscoplasticité. Cours C.I.S.M., No. 97, Springer Verslag, New York, 187 pp.

Molnar, P. and Tapponnier, P., 1981. A possible dependence of tectonic strength on the age of the crust in Asia. Earth Planet. Sci. Lett., 52: 107–114.

Tapponier, P. and Molnar, P., 1976. Slip-line field theory and large-scale continental tectonics. Nature, 264: 319–324.

Tapponnier, P., Pelzer, G., Le Dain, A.Y., Armijo, R. and Cobbold, P., 1982. Propagating extrusion tectonics in Asia. New insights from simple experiments with plasticine. Geology, 10: 611–616.

Tapponnier, P., 1977. Evolution tectonique du système Alpin en Méditerranée: poinçonnement et écrasement rigide-plastique. Bull. Soc. Geol. Fr., 3: 437–460.

Tapponnier, P., 1978. Les mécanismes de la déformation intracontinentale, exemple de la tectonique Alpine en Asie et en Europe. Theèse d'Etat, Montpellier, 460 pp.

Vilotte, J.P., 1983. Etude mécanique et numérique de deux types de mécanismes géophysiques de déformation inélastique: cas d'une collision continentale, cas d'évolutions postsismiques. Thèse de spécialité, Montpellier, 128 pp.

Vilotte, J.P., Daignieres, M. and Madariaga, R., 1982. Numerical modeling of intraplate deformation: simple mechanical models of continental collision. J. Geophys. Res., 87: 10709–10728.

Vilotte, J.P., Madariaga, R., Daignieres, M. and Zienkiewicz, O.C., 1984. Numerical study of a Continental Collision Process — Influence of the buoyancy forces and of an initial stiff heterogeneity on the evolution of intracontinental deformation. C/R/488/84, Institute for Numerical Methods in Engineering, Swansea, U.K. Geophys. J.R. Soc., submitted.

Zienkiewicz, O.C., 1977. The Finite Element Method. McGraw-Hill, New-York, 851 pp.